Functional Connectivity Network Analysis of Alzheimer and Mild Cognitive Impairment Patients

by

Duygu Şahin

B.S., in Physics, Middle East Technical University, 2010

Submitted to the Institute of Biomedical Engineering
in partial fulfillment of the requirements
for the degree of
Master of Science
in
Biomedical Science

Boğaziçi University
2014

ACKNOWLEDGMENTS

First, I would like to thank to my advisor Prof. Dr. Ahmet Ademoğlu for his support, consideration, and guidance through my study. He has made invaluable contributions in every possible way to my academic progress through the three years we have worked together.

Besides my advisor, I am sincerly grateful to Assist. Prof. Dr. Adil Deniz Duru for his support, guidance and encouragement. I fell honored to have a chanace to share his knowledge in a very inspiring, time and place limitless environment.

If without the insight and guidance of Prof. Dr. Tamer Demiralp, this thesis would not be possible. I am grateful for the opportunity he gave during but not limited with my internship.

I would like to express my gratitute to Assoc. Prof. Dr. Burak Güçlü, for his constructive view and contributions during my presentation. I would also like to thank Assist. Prof. Dr. Dilek Göksel Duru for her support and insight. For the inspirational discussions, I would like to thank Prof. Dr. Ata Akın.

I also feel very happy to have friends beyond friends, Evrim Aksel and Taylan Balcıoğlu, who support and encourage me tremendously.

Specially, I would like to thank my parents, Hale Şahin and İbrahim Şahin for giving me comfort and support unconditionally.

Lastly, I feel very lucky and proud to be a part of Neurosignal Lab at Biomedical Engineering Institute of Boğaziçi University.

ABSTRACT

Functional Connectivity Network Analysis of Alzheimer and Mild Cognitive Impairment Patients

In our era, while the life span is expanding, neurodegenerative diseases, such as Alzheimer's disease (AD), pose a great threat upon the quality of life. In such a case, the best course of action would be to detect, modify or treat the pathologies before they become too severe. Since the main cause of AD is still unknown, further studies for possible biomarkers are needed. Therefore, in this study, the objective is to find a distinctive agent for AD and mild cognitive impairment (MCI) from an optimized auditory oddball task fMRI data via functional connectivity analysis. In order to achieve that, a group ICA approach using temporal concatenation of the subject data is adopted. Since, there are no studies investigating functional connectivity of AD and MCI during an oddball task, especially via group ICA, this study can enrich the literature. As the results are concerned, in group comparisons, no significant differences are found in spatial maps. On the other hand, there are promising findings in temporal course analysis of the components such as the multiple regression outcomes. Therefore, our next aim will be to perform a longutidinal study including both resting state and task related data for finding a better biomarker.

Keywords: fMRI, Alzheimer's disease, mild cognitive impairment, independent component analysis, oddball paradigm.

ÖZET

Alzheimer ve Hafif Bilişsel Bozukluk Hastalarında Fonksiyonel Bağlantılılık Analizi

Çağımızda, insan ömrü gün geçtikçe uzamaktadır. Fakat, Alzheimer gibi nörodejeneratif hastalıklar hayat kalitesi açısından tehlike oluşturmaktadır. Bu tarz durumlarda, yapılabilecek en iyi şey hastalık çok ilerlemeden hatalığı saptamak, hafifletmek veya tedavi etmek olacaktır. Alzheimer'ın esas nedeni hala bilinmediğinden, olası biyobelirteçleri bulmak amacıyla yapılacak çalışmalar büyük önem taşımaktadır. Dolayısıyla; bu çalışmanın amacı, Alzheimer'ı ve hafif bilişsel bozukluğu ayırt edebilecek etkenleri optimize edilmiş oddball paradigması süresince alınan fMRG verisine fonksiyonel bağlantılılık analizi yaparak belirlemektir. Bunun için, zamansal olarak denek verilerini birbirine bağlayan bir grup bağımsız bileşen analizi yöntem olarak belirlenmiştir. Şimdiye kadar Alzheimer hastalığı ve hafif bilişsel bozukluğu olan kişilerin oddball görevi süresince çekilen fMRG verileri fonksiyonel bağlantılılık yönünden, özellikle de grup bağımsız bileşen analizi ile incelenmediğinden, bu çalışma literatüre katkıda bulunacaktır. Sonuçlar göz önüne alındığında, gruplar arası karşılaştırmalarda uzaysal haritalarda anlamlı bir değişiklik gözlemlenmemiştir. Buna nazaran, bileşenlerin zamansal seyirlerinin analizinde umut verici bulgulara rastlanmıştır. Bu bağlamda, bir sonraki hedef hem dinlenme halindeki hem de görevle alakalı fMRG verilerini içeren uzunlamasına bir çalışma yapmak olacaktır. Böylelikle daha detaylı bir biyobelirteç araştırması yapılabilecektir.

Anahtar Sözcükler: fMRI, Alzheimer, hafif bilişsel bozukluk, bağımsız bileşen analizi, oddball paradigması.

TABLE OF CONTENTS

LIST OF FIGURES

LIST OF TABLES

LIST OF SYMBOLS

A	The mixing matrix
B_0	Magnetic field strength
c	Component number
$CMRO_2$	Cerebral metabolic rate of Oxygen
c_{PCA}	Principal Component number
G_x	Reading gradient
G_y	Phase encoding gradient
H	Gaussian noise matrix
O_2	Oxygen
r	The correlation between two components
S_{ICA}	Source matrix
S_n	Total number of slices
$Subject_n$	Subject number
S_{V_n}	Total number of voxels in a slice
T_1	Spin-lattice relaxation
T_2	Spin-spin relaxation
T_2^*	Effective transverse relaxation
X_{CA}	Time series of voxels for component analysis
β	The amplitudes of the design matrix
ϵ	Noise process
γ	Gyromagnetic ratio
ω	Larmor frequency

LIST OF ABBREVIATIONS

AD	Alzheimer's Disease
ANOVA	Analysis of Variance
BOLD	Blood Oxygenation Level Dependent
CBF	Cerebral Blood Flow
CBV	Cerebral Blood Volume
CT	Control
DARTEL	Diffeomorphic Anatomical Registration using Exponentiated Lie algebra
DICOM	Digital Imaging and Communications in Medicine
EPI	Echo Planar Imaging
(f)MRI	(Functional) Magnetic Resonance Imaging
FWER, FDR	Family-wise Error Rate, False Discovery Rate
GE, SE	Gradient Echo, Spin Echo
GIFT	Group Independent Component Analysis
HRF	Haemodynamic Response Function
ICA	Independent Component Analysis
MANCOVA	Multivariate Analysis of Covariance
MCI	Mild Cognitive Impairment
MPRAGE	Magnetization-prepared Rapid Gradient Echo
MNI	Montreal Neurological Institute
NIfTI	Neuroimaging Informatics Technology Initiative
PCA	Principal Component Analysis
RF	Radio Frequency
SENSE	Sense Encoding
SPM	Statistical Parametric Mapping
SVD	Singular Value Decomposition
TR, TE	Repetition Time, Echo Time

1. INTRODUCTION

1.1 The Aim of the Study

In order to increase the life expectancy with adequate quality, research interests are focused on developing both diagnostic and prognostic biomarkers for the diseases. Undoubtedly, Alzheimer's disease (AD) is the most common type of dementia by affecting more than 50% of the elderly population [6]. Thus, it is one of the major research areas. However, the main cause of this ever growing disease is still a mystery. There are no exact distinguishing diagnostic methods as well as an effective modifying treatment [7, 6, 8]. The current methods investigating non-invasive techniques, have the focus on the resting state functional connectivity and effective connectivity of neurological disorders since 2005. The findings suggest that the disruptions in the networks have a pattern and sequence which are yet to be studied. Therefore, in this study, the aim is to find a biomarker for the discrimination of AD and MCI from each other as well as from healthy controls by a functional connectivity analysis. The novelty presented in this study is about the functional connectivity analysis of the AD and MCI data related with an optimized auditory oddball task. To our knowledge, there are no auditory oddball functional connectivity studies including both AD and MCI patients.

1.2 Mild Cognitive Impairment and Alzheimer's Disease

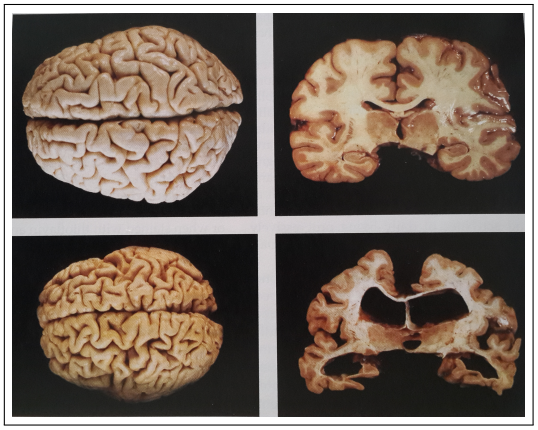

Figure 1.1 The difference between a healthy brain and a brain with Alzheimer's disease [1]

Mild cognitive impairment (MCI) is a syndrome which causes cognitive decline greater than the expected rate relating to age and educational level. However, it is not as severe as to effect daily life of a person. Moreover, it is also possible for this disease to stay stable or vanish over time in the best case scenario [9]. Nevertheless, with more than 50% probability, it can progress into dementia within five years [9]. Particularly, amnestic sub-type of this syndrome is known to convert into AD (thus referred as a prodromal stage for AD).

Alzheimer's disease (AD) is a progressive neurodegenerative disorder (Figure 1.1) which involves cognitive, intellectual and behavioural disruption [7]. The pathology in AD starts mainly in the hippocampus and entorhinal cortex, and subsequently spreads throughout most of the temporal lobe and posterior cingulate, finally involves extensive brain regions. Thus, the patient's abilities related to memory, attention, reasoning, language and executive functions become deteriorated gradually [6]. The main reason for these deteriorations are still an active area of research. However, current literature suggest that there are various reasons, some of which are related. These reasons are:

- Environmental factors such as toxins, viruses, prions, head trauma, low level of education [1].

- Aging and genetics [1, 10].
- Misfolded proteins such as β-amyloid that causes plagues and hyperphosphorylated-τ that causes neurofibrillary tangles (Figure 1.2) [1, 10].

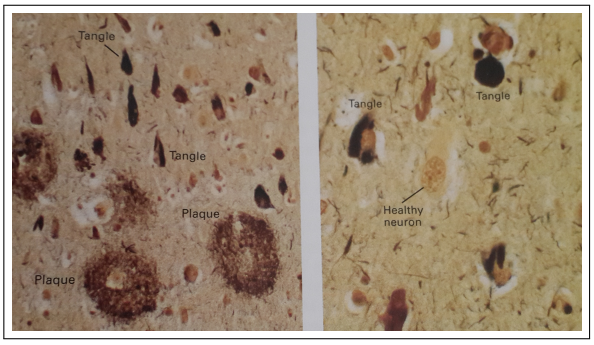

Figure 1.2 Plaques and tangles [1]

- Glucose hypometabolism [11] in areas either close or remote from amyloid toxicity. The low metbolism in amyloid free areas may be due to the reduced neuronal communication.
- Functional connectivity disruption [10] which can be explained by an extended version of disconnection syndrome as can be seen from Figure 1.3. According to this model, toxicity due to amyloid plaques and hyperphosphorylated-τ might disturb a brain region deteriorating the communication between other regions, but not severing them completely. Then the disease affects the regions either by the pathology extention due to structural connection or the bad signals due to functional connectivity.

In Figure 1.4, a summary of the current literature, also describing the relations between above mentioned changes can be found. According to the recent review article [10], in early stages of AD, salience network [12] and certain frontal regions show increased network connectivity either as a compensatory for the distrupted networks or due to amyloid excitotoxicity. However, as the disease progresses, the degradation in those networks occurs. Besides, in default mode network (DMN) (see Section 3.5), executive control network (see Section 3.2.2) and sensorimotor network (see Section 3.7) connections are found to be decreased for mild AD. These changes can be observed

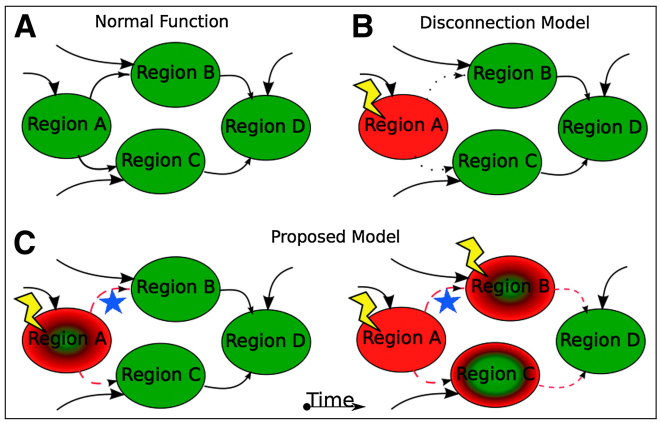

Figure 1.3 The suggested models for network disruption: A representing a healthy network, B representing disconnection syndrome model and C representing a recently proposed extended version of disconnection syndrome model [10]. The large arrows in the figure are depicting the inputs from other parts of the brain while the small arrows are for the communication between the regions shown in the figure. Green color is for a healthy region with intact connections shown by solid black lines. The pathology is shown by a lightning bolt affecting a single brain region and causing network disconnectivity (black dotted arrow) or disrupted but ongoing connection (dashed red arrow). The blue star stands for a structural connection which might allow the spreading of the pathology.

very early, even before the onset of AD if the genetic factors are present. It is also suggested that the disease starts with the degradation in DMN due to amyloid and τ deposition, then spreads to the other brain regions where no deposition is observed.

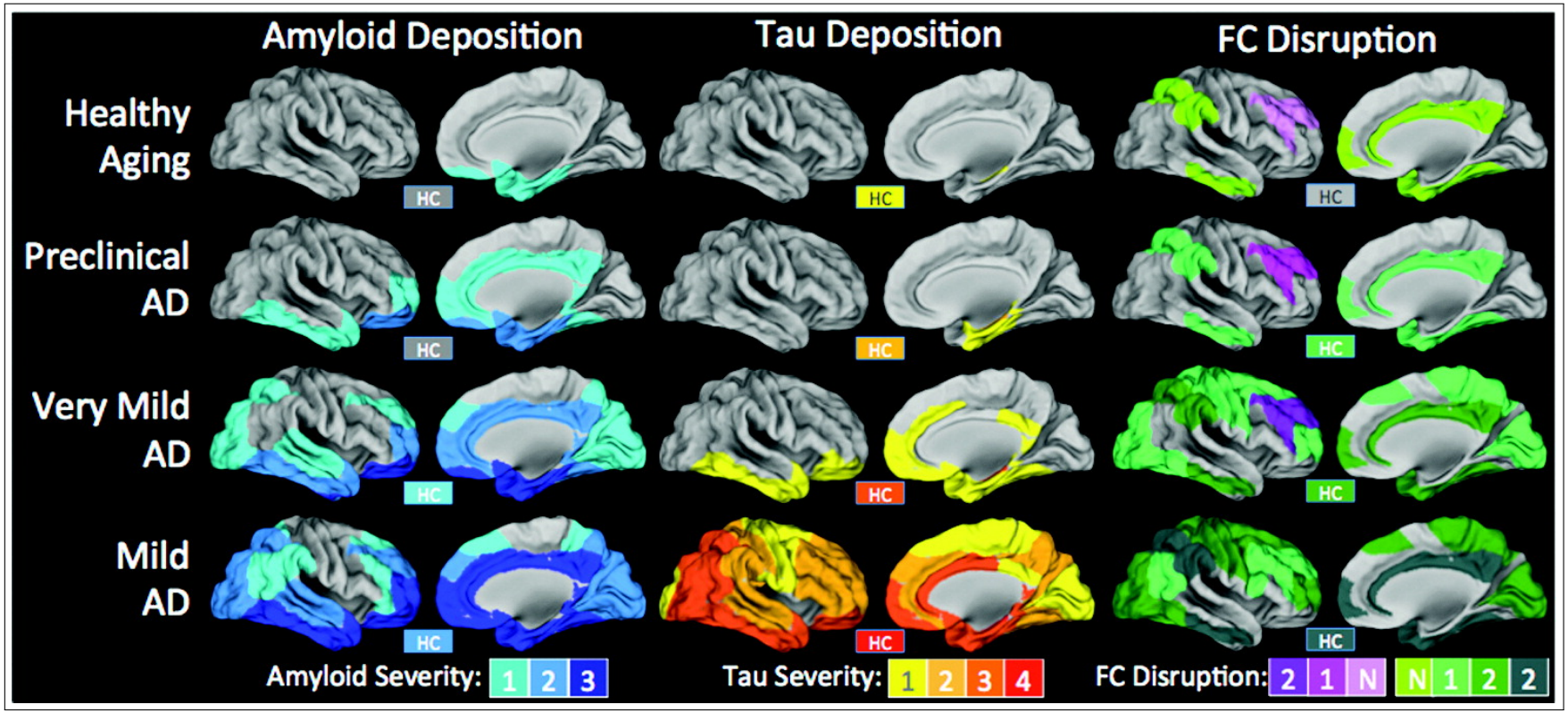

Figure 1.4 Summary maps of the studies about AD showing the extent and magnitude of amyloid and τ deposition and functional connectivity disruption parametric on disease severity [10]. Colors indicate the severity of deposits for amyloid and τ columns and a number of consecutive disease stages (in which greater abnormalities are detected) for functional connectivity column. The green-gray scale stands for functional connectivity loss whereas the pink-purple scale for functional connectivity enhancement. Since the hippopotamus is not visible on the surface projections, it is represented as a box labeled "HC".

1.3 fMRI Data

1.3.1 MRI and fMRI Data Acquisition Principles

Magnetic Resonance Imaging (MRI) is a cornerstone non-invasive neuroimaging technique for both clinical diagnosis and academic research. Primarily, the output is the structural image of the the organs created by utilizing the differences of the magnetic properties of the tissues. Information about the physico-chemical state, vascularization and perfusion of the tissues, blood oxygenation, blood volume and even water diffusion can be gathered utilizing this technique [13].

The basic principles behind this modality is about the intrinsic quantum mechanical property, called spin, of the particles. By virtue of the spin, particles also have intrinsic dipole moment. In the presence of an external magnetic field, as the particles tend to be in the lowest energy state, most of the magnetic dipole moments align in the direction of the external field. The others align themselves in an anti-parallel fashion; thus, have higher energy states. In the big picture, there is a net magnetization along the applied magnetic field. However, this alignment can be affected by the external magnetic field changes, magnetic moments of the particles due to their spins, magnetic fields due to orbital movement of the particles and their interaction with each other as well as electromagnetic waves capable of changing the energies of the particles [14]. In this system, one way to get information is to utilize magnetic resonance so that the particles can absorb electromagnetic energy and emit it to turn back to their stable form. This can be done via a radio frequency (RF) signal whose carrier frequency is equal to the Larmor frequency (ω) of the particle to be detected. The Larmor frequency (ω) depends upon the particle and the external magnetic field (B_0) through the gyromagnetic ratio (γ) ($\omega = \gamma * B_0$) [13, 15, 2]. Thus, it is possible to acquire signals from a desired particle as well as the location information by varying the parameters.

The basic theory behind the general mechanism can be understood via a simple imaging scheme. When the subject is put in the machine, the initial field is applied to make the net magnetization aligned in z direction (superior/inferior). Shortly after,

the RF is applied to tilt the net magnetization 90 degrees on x-y plane. At this stage, the spins begin to move coherently in phase as long as the RF is present. The period of RF is brief; thus, its effects on the net magnetization fade away (relaxations happen) in different time lengths depending on the tissue type. There are 3 types of relaxation processes, namely:

T_1 **(spin-lattice relaxation):** The duration needed for the relaxation of the longitudinal component (in the same direction of B_0) is called T_1 relaxation. This happens as the energy is released into the lattice, enabling the longitudinal component to become its maximum.

T_2 **(spin-spin relaxation):** The duration needed for the relaxation of the transverse component is called T_2 relaxation. This happens as the transverse component vanishes by releasing its energy to other spins due to the interaction resulting in phase incoherence.

T_2^* **(effective transverse relaxation):** Magnetic field inhomogeneity causes transverse relaxation time T_2 variation, which in turn results in the effective transverse relaxation, called T_2^*.

In order to encode the locations of the spins, small magnetic gradients are used additional to the B_0 magnetic field. Basically, during the RF, gradient in z-direction is applied for slice selection. Only the particles along that slice are affected as their Larmor frequency fit the applied RF. After the RF, gradient along the y direction is applied for a period to encode the direction with different phases (G_y, phase encoding gradient). Next, the acquisition is done while a gradient along x direction (G_x, reading gradient or frequency gradient) is on; thus, encoding the direction by the frequency. Naturally, the signals decay due to T_1, T_2 and T_2^* effects. As a result, a rephasing action becomes necessary for the quality and quantity of the signal. This can be done via various combinations of RF and gradient pulses, namely pulse sequences. Pulse sequences also define the contrast by reflecting the relaxation time effect by two parameters; the repetition time (TR) (defining how frequently the spins are excited)

and echo time (TE) (time delay between excitation and acquisition). For optimization purposes there are various kind of pulse sequences. Two of the main ones used for cognitive science are gradient echo (GE) or gradient recalled echo, using gradients to refocus the decayed signals and spin echo (SE), using RF to refocus the decayed signals. These sequences are also optimized for ultrafast imaging such as echoplanar imaging (EPI), spiral imaging and parallel imaging (including SENSE and GRAPPA), whose names describe the trajectories followed on k-space [13, 15, 2, 16]. By k-space, a Fourier space for the data to be stored is indicated. In Figure 1.5, k-space, which is sampled uniformly during acquisition, and image space with Cartesian coordinates, which is obtained after the inverse Fourier transform of k-space, is depicted. The spacing and sampling of the k-space plays an important role for the spatial extend and resolution of the image [3]. This is why it is optimized with different pulse sequences.

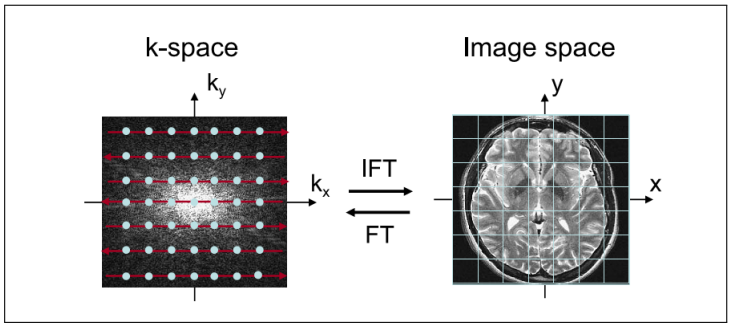

Figure 1.5 k-space and image space

In biological and clinical studies, hydrogen nuclei of water (a proton with spin 1/2), is mostly the source of the MRI signal since it is the most abundant element in tissues [13, 17, 15]. For structural MRI, the aim is to examine the anatomical features. Typical structural MRI consists of a T_1 weighted image separating gray and white matter clearly. On the other hand, T_2 contrast is good at separating fluids from tissues; thus, used for lesion and oedema detection. As for functional MRI (fMRI), the aim is to find the function related parts, neuronal populations, of the brain. Particularly, finding clues about top-down or bottom up regulations, inferring about cognitive capacity and defining biomarkers for the diseases from the spatial or temporal differences among groups of people are of interest. This can be done by measuring haemodynamic changes

with T_2^* contrast [13, 17, 15, 2].

1.3.2 BOLD Effect and Haemodynamic Response Function

Haemodynamic changes are usually traced with the oxygenation of blood as the relaxation time differs between diamagnetic oxyhaemoglobin (locally decreasing the magnetic field) and paramagnetic deoxyhaemoglobin (locally increasing the magnetic field). The chief assumption establishing the adequacy of this measurement to infer about neuronal activations is that the neurons need more oxygen when they are activated and this need is compensated by the increase of the blood flow. In the bigger picture, the need of energy leads to enhanced glucose utilization with oxygen; however, the oxygen consumption rate (cerebral metabolic rate of O_2 utilization $CMRO_2$) falls beyond the carried O_2 via the increased cerebral blood flow and this results in the deoxyhaemoglobin decrease [13, 2].

The contrast depicting the difference between blood oxygenation is specially named as blood-oxygen-level-dependent (BOLD) contrast. The function modeling the changes in BOLD after a stimulus induced or spontaneous neuronal activation is called the haemodynamic response function (HRF). As can be seen in Figure 1.6, with the increase in $CMRO_2$, there is an initial dip followed by a positive BOLD with the rise of cerebral blood flow (CBF) as well as the cerebral blood volume (CBV). After 10s, CBF and $CMRO_2$ turn back to their baseline states. Since the CBV return is slower, it aids in signal drop due to the building concentration of deoxyhaemoglobin. In the canonical model of the HRF, the initial dip is not considered as it is invisible at low field strengths. Apart from canonical model, there are various models enabling flexible parameter choices according to the study [3, 18, 19, 2]. Since there are many unknown issues about brain dynamics, HRF modeling is an active research area with the aspects of neurovascular coupling.

The BOLD can be affected in a confounding way from breathing patterns, drugs and substances (like caffeine, and nicotine), age and brain pathology, local differences

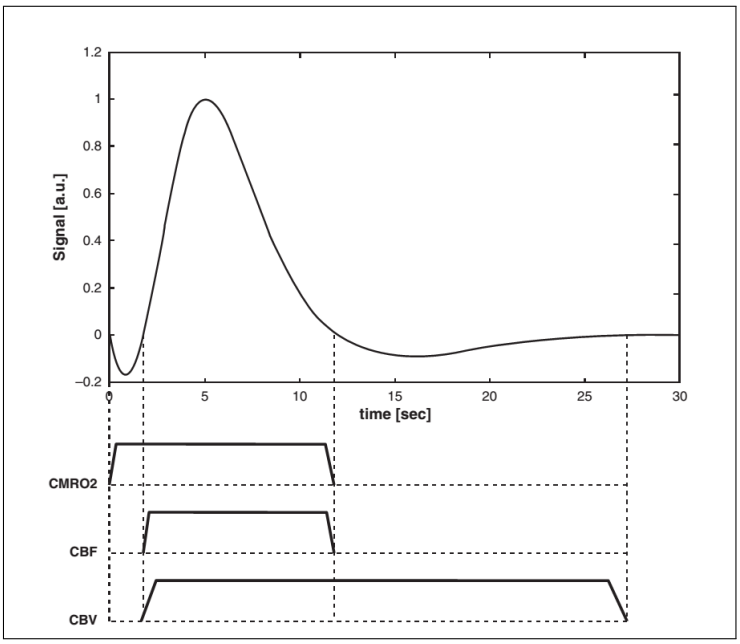

Figure 1.6 A typical haemodynamic response function with different time constants of the underlying physiological parameters [2]

in neurovascuar coupling, attention, excitation and inhibition [17]. This is due to the vulnerability of brain perfusion towards external and internal environment and the mostly unmeasured effect of the amount and diverseness of neurovascular coupling in a subject and between subjects. Beside the physiological signals, motion of the subject causes signal blurring as well as spurious activations. Apart from subject related effects, the machines and the agorithms also cause problems such as ghost artifacts, ringing effect, signal drop-out due to thermal motion of electrons and spurious activations due to wrong or deficient modeling [3].

1.3.3 Experimental Designs

There are two classic experimental designs, namely block and event-related designs (Figure 1.7). As the name suggests, there is a sustained action period as well as a no-action period for a block design. On the other hand, for an event-related design there are recurring on and off sessions, which are usually a lot shorter than a block in the former design. The designs are mostly optimized according to HRF. This is peculiarly important for event-related designs when a linear relation between stimuli

and BOLD response is required. Naturally, both designs have upsides and downsides. The prolonged activation in the block design provides higher BOLD signal as well as sound to noise ratio. However, the temporal information is not as detailed as for the latter design. Experiments can be shorter if block design is used, but for an experimental design, there has to be large samples with adequate interstimulus intervals [3, 17]. It is also possible to overcome long experiments by using rapid jittered protocols or de-convolution analysis methods if they are suitable for the study [17].

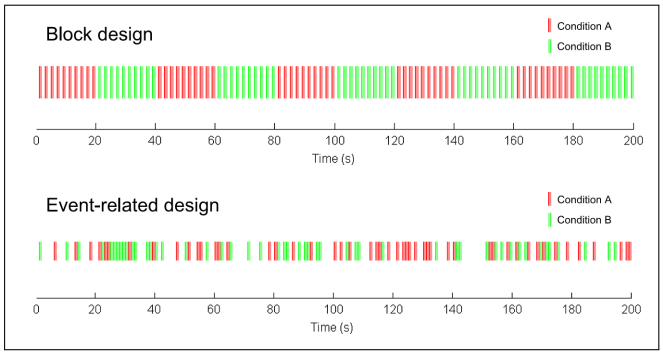

Figure 1.7 Block design (top), event related design (bottom) [3]

There is one more possibility for an fMRI study, which is to image the spontaneous activity of the brain. This kind of study is called a resting state study [20], and it gained popularity recently for its potential in distinguishing disease related conditions.

1.3.4 Structural and Statistical Properties of fMRI Data

Typical fMRI image contains a structural image obtained at the beginning for anatomical details and a functional image for dynamic details. In Figure 1.8, a simple visualization of fMRI data can be seen.

Generally, whole brain volumes are taken in various time points, which are usually separated by time of repetition (TR). Each of the volumes consists of voxels which are simply the volume units. The values of the voxels, the intensities recorded, depend on the image contrast chosen such as T_2^*. In Figure 1.8, the graph at the right bottom reflects the time course of one voxel which is repeatedly imaged for N times.

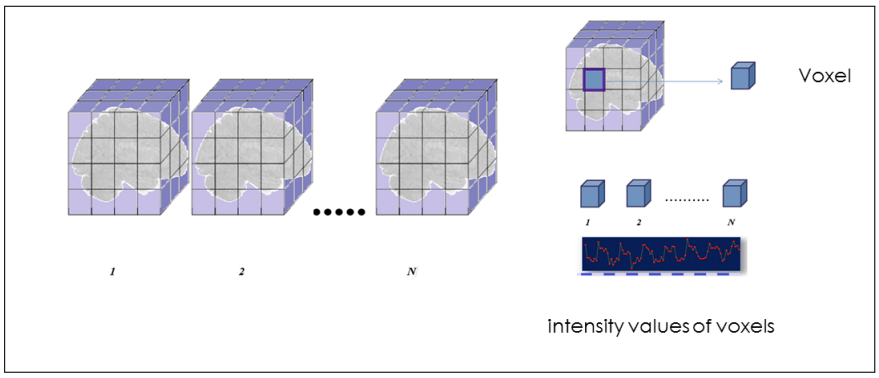

Figure 1.8 fMRI data structure

There are $N \times S_{V_n} \times S_n$ times of time courses for an fMRI data, where S_n is the number of slices and S_{V_n} is the total number of voxels in a slice. Thus, there are two kinds of information for each voxel at each time point, one for the location and one for the time point value. Totally, this makes a 4D data consisting of 3D localization information and time series information. For computational reasons, the data can be stacked in various ways such as in 4D and in 3D. Moreover, the methods include several header information or other related metadata encoding techniques. The most common stacking formats are Analyze and NIfTI (Neuroimaging Informatics Technology Initiative) in the neuroimaging community [1] .

The fMRI data can give a high spatial resolution relative to other modalities measuring brain dynamics. The average voxel size used before any preprocessing is reported to be 55 mm^3, encapsulating 5.5 million neurons in human brain [13]. However, haemodynamics and machine design limits the maximum temporal resolution that can be obtained. The TR range for most of the studies changes between 0.5 to 4 seconds, where 2 seconds deemed adequate for the observation of activation patterns which can be explained by HRF.

Usually, a typical study consists of 100 to 2000 brain volume images with approximate dimensions of $64 \times 64 \times 30$ for each subject session. Roughly, each of the 122.880 voxels have a size of $3 \times 3 \times 5$ mm^3. The session and subject number depends on the research, but at least 10 to 40 is required for a population inference [3, 21]. The

[1] The details can be found at http://nifti.nimh.nih.gov/.

fMRI data, BOLD response captured with noise, relatively reflects assembled activity of neurons. Unfortunately, it has a complicated spatio-temporal correlation for each subject. In order to get relevant and accurate results from the data, it is crucial to understand the nature of the data via statistics. Below is a summary of distribution statistics for each step of (f)MRI data:

Difference between the spins parallel and antiparallel to B_0: Follows a Boltzmann distribution, and the difference increases with the field strength [13].

Raw k-space data, thus the reconstructed data: They have normally distributed complex values with independent normally distributed error ($Value = R+I+E$) [3].

The magnitude of k-space data (In most studies only magnitude is used, phase is discarded): Follows a Rice distribution. If there is no signal, it converges to Rayleigh distribution; however, if sound to noise ratio is high, it converges to Gaussian distribution [3].

1.4 Preprocessing of fMRI Data

As mentioned before, fMRI signal is a combination of a relatively weak BOLD signal and spatiotemporal noise creating a complicated autocorrelated structure. Therefore, various preprocessing steps are necessary to obtain the signal which satisfies the statistical assumptions necessitated by the analyzing techniques and tests. Moreover, for group-wise comparisons, it is essential to match the locations of brain regions in order to get valid and sensitive results. Thus, preprocessing is an important step for obtaining cleaned and standardized data. Frequently used techniques [3, 15], which are prospective unless stated otherwise, are:

Slice timing correction: Each brain volume in fMRI is assumed to be imaged as a whole so that the acquisition time of each slice in a volume is equal to one another.

However, the timings depend on the k-space sampling method of acquisition. This creates a difference in time courses as they correspond to different conditions in the experiment. Consequently, the severity of the situation is more pronounced in studies using experimental designs. Thus, the timings of the voxels should be shifted or interpolated to match with each other. This step can be applied before or after the motion correction depending on the severity of the motion of the patients and the experimental design (However, there is still an ongoing debate about the sequence of this step).

Motion correction: One more assumption about the fMRI data is that each voxel corresponds to the same location for every volume. As the experiments take time, the subjects move during acquisitions. This change the locations of the voxels taken, and causing contamination of voxels by the other voxel signals; thus, leading to spurious activations. The classic way of realigning the data, if the movement is not too severe, is by using 6 degree of freedom rigid body transformation (including 3 translation and 3 rotation parameters) and a cost function to be minimized such as sums of squared differences. After the correction, the volumes having movements exceeding 1 or 2 times the voxel size or above 3 to 6 degrees of rotation can be discarded or the motion parameters can be used in further processing steps. The best is to acquire the cleanest data possible since current prospective algorithms are not sufficient enough to cope with the contamination [22]. For that, there are ways to minimize the movement inside the MRI scanner like using head fixation devices. There are also some retrospective methods such as capturing the position via a camera and correcting the misalignment online.

Coregistration: As the fMRI data is poor in detailing the anatomy, the results are usually mapped on the structural image for presentational purposes. In order to achieve that, the structural and functional images are aligned via rigid body (6 degree of freedom) or affine (12 degree of freedom) transformations. Before this step the structural images are segmented into parts like scalp, skull, gray matter, white matter and cerebrospinal fluid. Some studies also include skull stripping before any process is done to structural images in order to get better results at

this step.

Normalization: In order to do group comparisons, there needs to be a standardization for the brain structures. This is done by normalization of the subject brains to previously created templates such as Talairach or Montreal Neurological Institute (MNI)brain with non-linear algorithms. (For better results, the templates can be generated from the subjects if the numbers are enough or other population specific templates such as the ones for elderly people or Asian people can be used if they fit better for the study.)

DARTEL (Diffeomorphic Anatomical Registration using Exponentiated Lie algebra): It is an image registration algorithm developped by John Ashburner. It has an efficient diffeomorphic framework optimized by a Levenberg - Marquardt strategy [23]. Recently a more mathematically correct version using large deformation diffeomorphic metric mapping with Gauss-Newton optimization algorithm is presented [24] (but it is still in progress for usage as a toolbox). In studies, it is found that DARTEL has better results when compared to classical methods [25]. Especially in one Alzheimer voxel based morphometry study [26], it is though to enhance the process. It is also possible to create templates from subjects' data with this algorithm.

Spatial smoothing: fMRI images are usually smoothed via a Gaussian kernel of 4 to 12 mm full width half maximum. This enhances the normalization via blurring out subjective anatomical differences and increases the signal to noise ratio by reducing the random noise in individual voxels. Moreover, a kernel with full width half maximum of 3 to 4 times of voxel size is needed to smooth the data to fit the assumptions of random field theory which will be elaborated later [3].

Additional procedures: According to the needs of the research, some additional procedures can be applied in the preprocessing or processing step by considering the bias imposed on the data. Some of these procedures are deskulling of the structural data [27], intensity correction of the structural data [28], despiking the temporal course [29], removal of realignment outliers via scrubbing them out

or regression [30], ventricle masking to avoid ventricular activations [29], band-pass filtering [29], global parenchymal signal removal [22, 29], PCA, ICA, and retrospective methods [31]. In Table 1.1, some preprocessing techniques for the noise removal are described.

Table 1.1
Noise in fMRI data and possible preprocessing methods to cope

Subject related noise:	by PCA, ICA, wavelet analysis,
Cardiac (0.6-1.2 Hz)	filtering, retrospective methods, modelling
Respiratory(0.1-0.5 Hz)	filtering, retrospective methods, modelling
Movement	realignment , scrubbing, reggressing out
Scanner related noise:	by filtering, regression,intensity correction
Drift (low frequency noise)	
Random noise (independent of task, no spatial structure) due to thermal motion	

1.5 Functional Connectivity

Brain consists of an efficient network with functional and anatomical connections of spatially distributed areas [32, 33]. In this context, for information sharing, three types of connectivity can be distinguished as anatomical, functional and effective [32, 3]. While anatomical connectivity refers to physical connections of various brain regions, functional connectivity indicates dynamic interactions of these regions such as their temporal dependency on each other [32, 33]. Anatomical connectivity and functional connectivity are mutually interdependent; however, the extent of this dependence is still studied for finding shaping and constraining networks. So far, it is presented that resting state functional connectivity mostly reflects the structural connectivity. However, functional connectivity patterns can be seen when there is no structural connectivity, which can lead to a conclusion that there might be a third location linking the connected parts [34]. As for the effective connectivity, directed interactions between the brain regions; thus, patterns of causal influence, are the main issue [32, 33]. In this study, functional connectivity will be studied as it provides comprehension about large-scale neuronal communication and how this connectivity and information integration relates to human behavior. Specifically, the importance also comes from the point that functional connectivity is likely to be the indicator of the quality and quantity of complex cognitive processes [33]. Therefore, hints about neurodegenerative diseases like AD and MCI can be obtained as mentioned in the subsection of MCI and AD (1.2).

1.5.1 Functional Connectivity Analysis Methods

In order to carry out functional connectivity analysis, deviations from statistical independence are assessed by estimating the correlation or covariance, spectral coherence, or phase locking between pairs of time series [32]. Some of the main methods developed for these processes can be divided into two groups as model dependent and model free [33, 3, 35, 36].

Model dependent methods, as the name suggests, construct a prototype of the BOLD signal as close as to the observed signal by the known and unknown parameters. The main model dependent methods are:

General Linear Modeling (GLM): In this model, time series of each voxel is regenerated via the assumed to be known BOLD response and noise model. Then the residual error is minimized mostly by generalized least squares. This is the first level where each subject's data is considered. There is also a second level where group differences can be modelled.

Seed Based Methods: For this method the first step is to determine a seed, which can be a voxel, a region, a performance or a physiological variable. After selecting the seed, additional preprocessing steps might be used to obtain relevant fMRI BOLD signal. Then the brain regions related with the seed by passing a relevant threshold are found via cross correlation, phase coherence or GLM fit [3, 36].

Model free methods do not assume anything about the response mechanism, they drive the results from the data. The main model free methods for functional connectivity analysis are:

Principal Component Analysis (PCA): The aim of this method is to find spatial patterns with greatest amount of variability in their time series. Thus, eigen-images ordered by the variation they convey are computed via singular value decomposition (SVD) or eigenvalue decomposition.

Independent Component Analysis (ICA): Aim of this method is to find either spatially or temporally independent, nonlinearly uncorrelated [37], components. This is obtained either by minimizing the mutual information between components or maximizing the non-Gaussianity of the data [38].

Clustering Based Methods: The aim of this method is to combine voxels into clusters according to their time series' similarity described by the distance metric [36].

1.5.2 Method Selection

Each technique investigating functional connectivity needs expertise for careful enough designing. Whether the study is task related or resting state network assessment, the above mentioned methods can be used [39, 40, 41, 42] and results consistent with the relevant literature can be obtained. Among functional connectivity studies, GLM and ICA are the most popular techniques so far. For GLM, the quality depends on the model parameters and algorithms chosen. In order to avoid any prior information about the data, decomposition methods are usually preferred. PCA is mostly used only for preprocessing as it is inefficient for functional connectivity analysis. This is due to the second order statistics utilization and linear independence assumption of PCA. Based on the study and survey on the analysis methods, ICA is chosen. The reasons for this approach to be the one for this thesis can be summarized as:

- To avoid mismodeling either by using too many priors or overlooking the parameters,
- To avoid seed selection and related problems such as time variance of the response and erroneous correlations,
- To benefit from ICA's increased sensitivity to detect subtle differences between subjects when compared to seed-based methods [43],
- To benefit from ICA's popularity and validity; thus, the broad range of literature on the topic,
- To search the content of the data in this study, as consensus was made on the appropriateness of ICA.

1.5.2.1 ICA. In Figure 1.10, the equation for spatially independent components can be seen as $X_{CA} = AS_{ICA}$, where X_{CA} represents the data, A ($T \times c$ matrix) represents the mixing matrix or the time courses of the spatially independent components, and S_{ICA} ($c \times N$ matrix) is source matrix containing spatially independent

components. If the inverse of the data matrix is used, temporally independent components are found. In this equation, A and S_{ICA} are unknown. Thus, the problem (blind source separation) turns into finding the best unmixing matrix, A^{-1} for equation $S_{ICA} = A^{-1}X$ iteratively, so that the components are maximally independent from each other [4]. This can be done either by minimizing the mutual information between components or maximizing the non-Gaussianity of the data [38]. Thus, the algorithms are separated into two main groups as the ones using mutual information minimization (i.e. Infomax algorithm [44]) and the ones using kurtosis or negentrophy for non-Gaussianity maximization (i.e. FastICA algorithm [45]). For these methods to be applied, the assumptions to be met are:

- **Non-Gaussianity of the data:** As can be understood from the methods, the components in the source matrix are thought to be statistically independent and linearly mixed by the mixing matrix elements. In order to find the best unmixing matrix providing the independence of the components, the distribution of the data should be non-Gaussian. As can be seen from Figure 1.9, non-Gaussianty provides information about the mixing matrix as the joint distribution of the sources becomes non-symmetric.

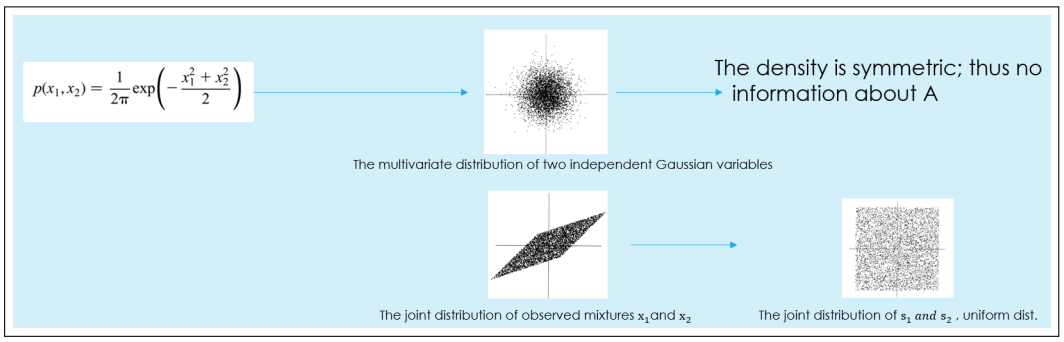

Figure 1.9 Example about the joint distributions of Gaussian and non-Gaussian parameters [4]

- **Independence of the components:** As this is the aim of the method.
- Full rank and square A: A should be full rank and square for simplicity. However, it can be relaxed if necessary [4].

For these assumptions to be met, data should first be centered (made 0 mean) and whitened (sphered/ forced to be uncorrelated). After these steps, reduction should be done by PCA in order to decrease the computational load. A nice demonstration of ICA by FastICA algorithm can be found at the website http://research.ics.aalto.fi/ica/icademo/.

Up to this point, the only source of stochasticity was the source matrix. There is also one more type of ICA analysis called the probabilistic ICA (PICA), which incorporates Gaussian noise into the picture ($X_{CA} = AS_{ICA} + H$) [46, 47].

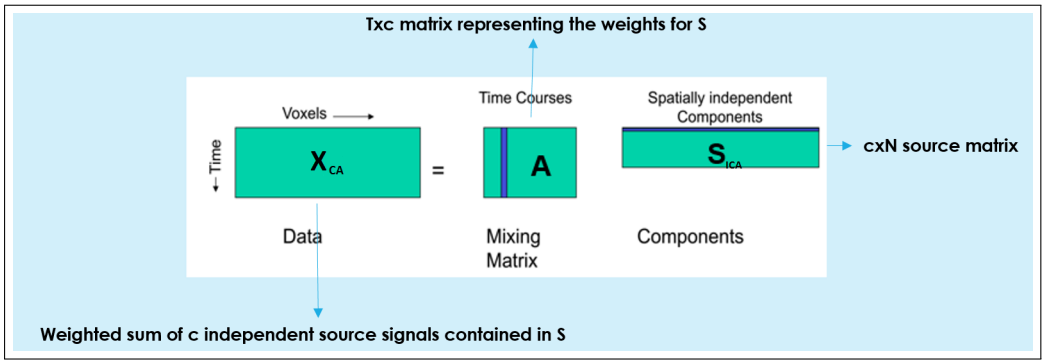

Figure 1.10 Independent Component Analysis

There are various ways for performing group inferences with (P)ICA [48]. In this study, GIFT software is chosen for its compatibility with Matlab and the technique it uses for group inferences. This choice is also based on the literature [43, 48, 49, 50, 51, 40] comparing various methods and algorithms, and indicating that using ICA with temporal concatenation as well as GICA3 back-reconstruction algorithm gives the best results for resting state functional connectivity studies. Since this analysis is also valid for task related fMRI data [40], the details described are used in this thesis.

1.6 About Statistical Correction Methods

The outcome of fMRI study usually involves a statistical parametric map (SPM) depicting the brain activity via color codes painting the significant voxels according to some statistical threshold (usually t-value). The threshold is supposed to reflect the

balance between sensitivity (true positive rate) and specificity (true negative rate). At the same time, as the tests are done simultaneously for each voxel, adding up to 100.000 voxels for each volume, it is important to correct for multiple comparisons. There are various ways which differ in the error rate they control, such as family-wise error rate (FWER) and false discovery rate (FDR) [3, 52].

Family-wise Error Rate (FWER): It is the probability of false positives (Type I errors, Figure 5.1) in a family of tests, under the null hypothesis. The methods correcting for this kind of error include Bonferroni, random field theory and permutation tests.

1. Bonferroni is too conservative as it assumes that all voxels are independent from each other. However, there is an inherent dependency due to spatiotemporal autocorrelations in fMRI data as well as neighboring voxel dependency [17]. This method; therefore, decreases the power of the test, which means that the probability of accurate rejection of a false null hypothesis drops. At the same time, false negative rate may increase.
2. With the help of Gaussian Random Fields theory, higher order statistics can be applied at voxel level or cluster level thresholding with accounting for the spatial correlation. However, this method is also very conservative and it necessitates the images to be a derivative of multivariate Gaussian images as well as to be sufficiently smoothed (like 3 or 4 times the voxel size).
3. Non-parametric methods, like permutation tests, can be used without making any assumptions about the distribution of the data. Also, they are found more successful to control FWER especially with small sample sizes [17, 3].

False Discovery Rate (FDR): Proportion of false positives among rejected tests are controlled by FDR. Tests are mostly assumed to be independent when they are dependent. Thus, incorporation of spatial information should be developed. In the case the null hypothesis is true, FDR becomes equal to FWER. Procedures controlling the FWER can also have control over FDR. However, procedures specific to FDR are less stringent; thus, resulting in power rise. Moreover, the

control mechanism only works with p-values; therefore, can be applied to any statistical test [17, 3, 52].

2. SUBJECTS and METHODS

2.1 Subjects

Total of 16 subjects (5 AD, 6 MCI, and 5 CT) are chosen among 64 subjects (17 AD, 34 MCI, and 16 CT) according to their ages (68 as average), the goodness of their structural MRI and functional MRI. Subjects having ages in the outlier range and/or bad scans as in Figure 2.1 are eliminated for refined results. The bad scans in Figure 2.1 include lost superior or temporal brain parts due to the field of view shifts (MCI Subject 08), signal loss due to tooth implants or machine caused reasons (Alzheimer's Subject 08 and MCI Subject 05), fixable bad normalization due to disorientation of the scans (Alzheimer's Subject 09) and age and/or disease related big ventricles (MCI Subject 03).

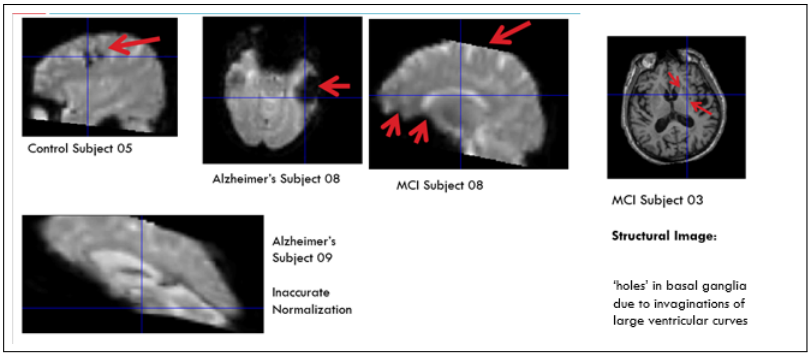

Figure 2.1 Bad (f)MRI scans of subjects

2.2 Methods

2.2.1 Experiment Paradigm

As the experiment paradigm, an auditory oddball paradigm variant whose intervals between the stimuli are specifically optimized for event related fMRI measurements is used. Classically, in an oddball paradigm, randomized target stimuli having 1500

Hz frequency are placed with 20% probability between 1000 Hz standard sounds. The stimuli have a duration of 200 ms, and an inter-stimulus interval of 2 $secs$. The participants are supposed to press the button as fast as possible when they hear the high-pitched sound. In this experiment, the optimization is done by Opt-Sec program (http://www.opt-sec.com/) on the inter-stimulus intervals such that their minimum length becomes 1.2 $secs$. whereas their mean becomes 2.2 $secs$.

2.2.2 fMRI Data

The fMRI is taken via a $1,5$ T MR scanner (Achieva, Philips Healthcare, Best, The Netherlands) with SENSE-Head-8 coil at NPISTANBUL Neuropsychiatry Hospital, İstanbul. T_1-weighted MPRAGE sequence is employed as high resolution anatomical scan (voxel size $1.25 \times 1.25 \times 1.2$ mm; 130 slices; field of view 240 mm). After the 20 minute anatomical scan, a dynamic T_2^*-weighted gradient echo planar imaging sequence with 275 dynamics is used for BOLD measurements. Additionally, two other dynamics, usually not used for analysis of the steady state tissue magnetization, are added in front of the sequence. Functional EPI volumes are gathered using anterior commissure - posterior commissure aligned 26 axial slices with slice thickness of 4 mm without gap and field of view 230×230 mm ($matrix = 64 \times 64$ voxel) covering whole cerebrum. RT is 2400 ms with 50 ms echo time (TE).

2.2.3 Preprocessing

All preprocessing steps are carried out using Matlab 8.2 (R2013b) with Statistical Parametric Mapping toolbox (SPM12bhttp://www.fil.ion.ucl.ac.uk/spm/software/spm12b/). In order to use the toolbox, the DICOM files taken from the MR machine's software are converted into Nifti-1 (Neuroimaging Informatics Technology Initiative) format (in which one Nifti file exist per time point) via MRIConvert software (http://lcni.uoregon.edu/~jolinda/MRIConvert/). In order to get more accurate results in the proceeding steps, the data are skull-stripped first by watershed algorithm in

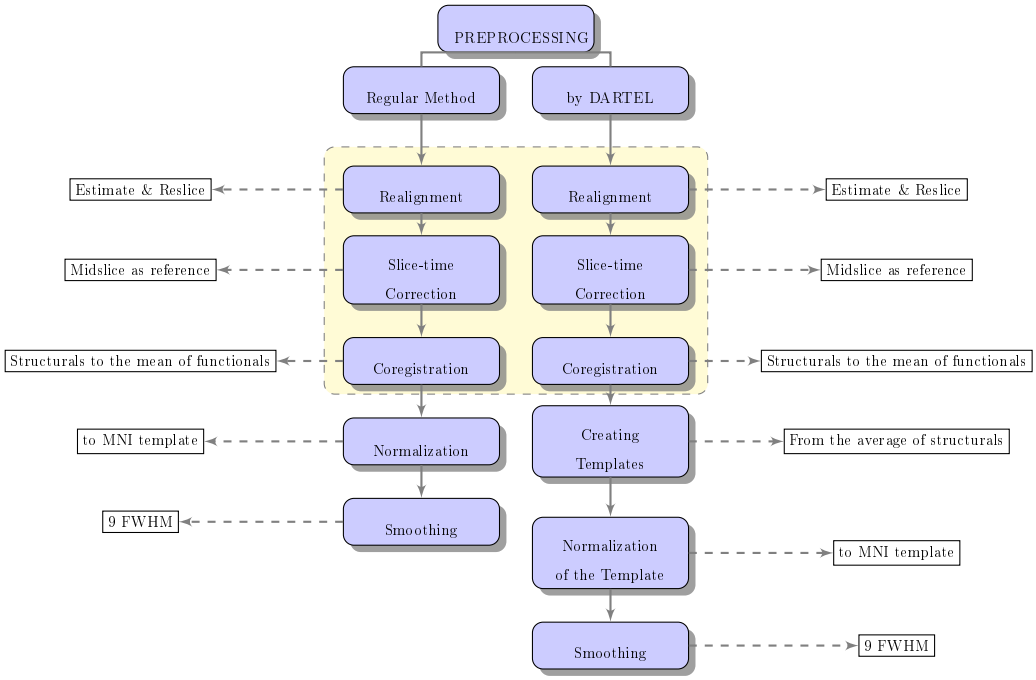

Figure 2.2 Preprocessing pipeline

FreeSurfer v5.3.0 (http://surfer.nmr.mgh.harvard.edu/) and later by BrainSuite v.13a4 (http://brainsuite.org/). Then, with SPM12b two different preprocessing steps are applied on the data separately as can be seen in Figure 2.2. Namely:

1. **Regular method:** Realignment, slice time correction with the middle slice as the reference slice, co-registration of the structurals to the mean of the functionals, normalization to the MNI template and smoothing with 9mm FWHM Gaussian kernel.

2. **DARTEL method:** Realignment, slice time correction with the middle slice as the reference slice, co-registration of the structurals to the mean of the functionals, creating a template from the average of the structurals with DARTEL toolbox of SPM12b, normalizing the template to MNI template and smoothing by DARTEL.

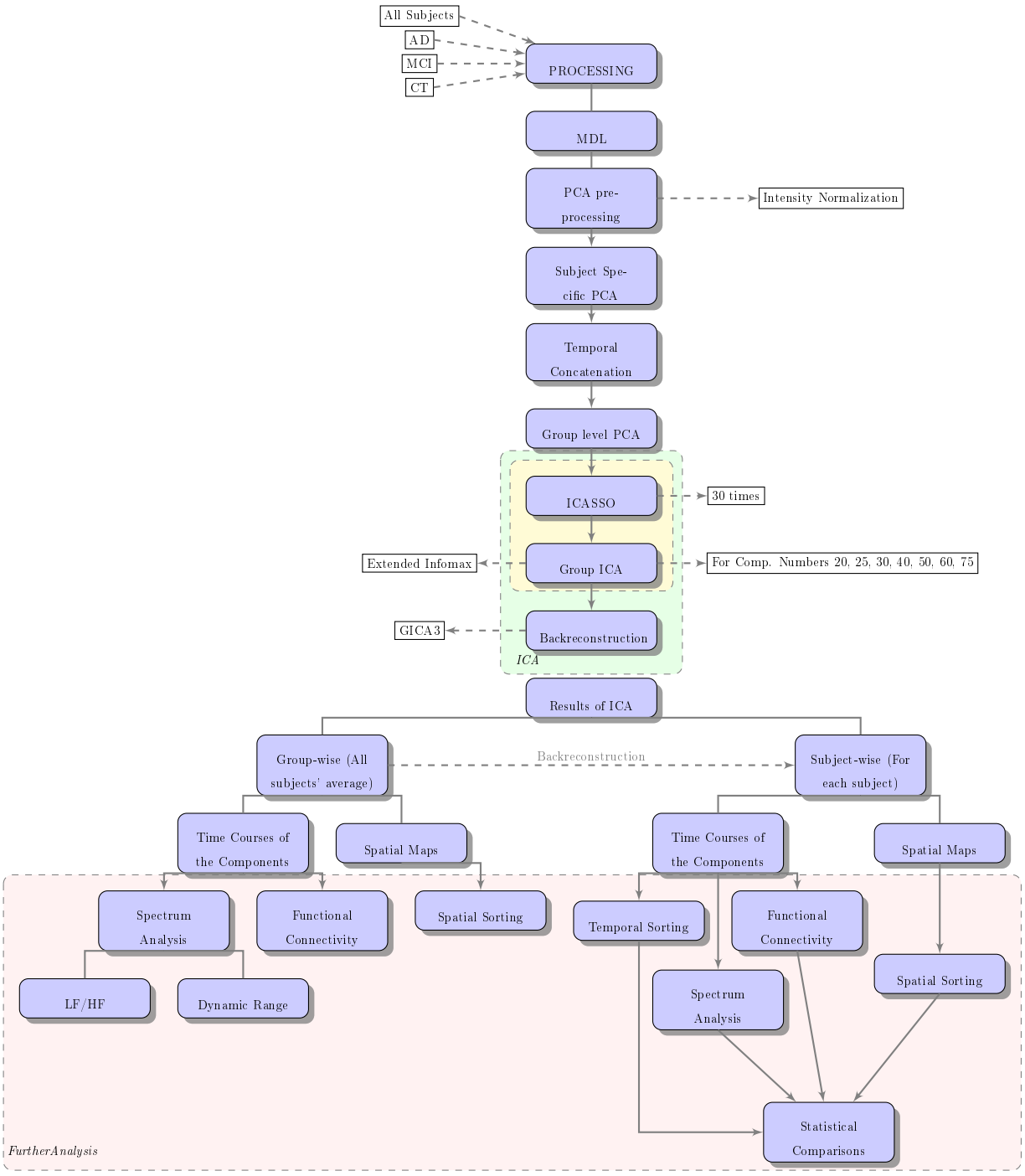

Figure 2.3 Processing pipeline

2.2.4 Processing

Data processing is done with Matlab 8.2 (R2013b), Group ICA Toolbox from MIALab (GroupICATv3.0a http://mialab.mrn.org/software/#gica) and Statistical Parametric Mapping Toolbox (SPM12b http://www.fil.ion.ucl.ac.uk/spm/software/spm12b/). The preprocessed data of subjects are put as inputs in two different ways for group inferences. For the first trial, all of the subjects are processed together whereas the groups (AD, MCI and CT) are processed in separate sessions for the second trial. As an additional step to the processing, minimum length description criteria (MDL) [53, 54] is used for all subjects to search for the maximum independent component number that can be get from the data. The processing pipeline, Figure 2.3, begins with intensity normalization (in which the time series are scaled into percent signal change). It is applied on the fMRI data as a preprocessing step of PCA. Next, the data is reduced with two step Principal Component Analysis (PCA). In the first step, subject specific PCA is done to get principal components, $1,5 \times c$. The reduced data, $c_{PCA} = Subject_n \times (1,5 \times c)$, are then whitened and temporally concatenated. Thus they become one group instead of as many as the number of subjects. For the second step, the temporally concatenated data are reduced into the number of chosen independent components via the group level PCA. After PCA, independent component analysis (ICA) is applied with the extended Infomax algorithm, 30 times with the help of ICASSO. In ICASSO, the infomax algorithm is run each time with both bootstrap and random initial points. As a result, spatial maps and temporal courses of the spatial maps as many as the chosen number of ICs are gathered in each time the algorithm is applied. The maps, $30 \times c$, are clustered by group-average linkage agglomerative hierarchical clustering. The centroids are then chosen as the most stable components and put into further analysis. In order to reach to the subject level, back-reconstruction algorithm GICA3 is applied on the centroids. After this step, both group-wise (average of all the subjects') and subject-wise spatial maps and their temporal courses are obtained.

For further analysis, the spatial maps of the group-wise ICs are sorted via visual inspection with respect to the literature. For the first trial, the group network name

of each component is automatically the same for all of the the subjects. However, for the second trial, in which each group is processed in a different session, the networks should be matched among the groups. After the identification of networks, subject's spatial maps are statistically analyzed with contrasts differentiating between AD, MCI and CT via ANOVA and MANCOVA analysis.

As for the TCs; three different processes - such as spectrum analysis, functional connectivity and temporal sorting - are carried out. First, spectrum analysis is applied on group-wise despiked, filtered (Butterworth filter with low-pass cut off 0.2 Hz) and baseline corrected TCs as well as despiked, filtered and detrended TCs. Three outputs for each measure are obtained as power spectrum, dynamic range and low frequency power integral to high frequency power integral ratio of the components. For dynamic range, the difference of the peak power with the lowest power in the frequencies after the peak power frequency is used. As for the low frequency range, spectral power below 0.1 Hz is used whereas spectral power above 1.5 Hz till 2 Hz is assumed to be in high frequency range. Second, the connectivity between networks are estimated in a pairwise fashion via Pearson's correlation between despiked, filtered and baseline corrected TCs. Then, the functional connectivity map is obtained via transforming the correlations into z-scores (with Fisher's transformation $z = atanh(r)$, where r is the correlation between two components). The first two methods are also done in a subject-wise fashion in order to compare AD, MCI and CT groups with MANCOVA. Third, subject's TCs are temporally sorted via multiple regression with the canonical HRF and time derivative of HRF convolved target signal, and normal signal (Figure 2.4). This is done in order to find the modulation of task in functional connectivity networks. Moreover, statistical tests are done on β values (4 different values for each subject) with various contrasts (Figure 2.5) selecting regressors and/or groups.

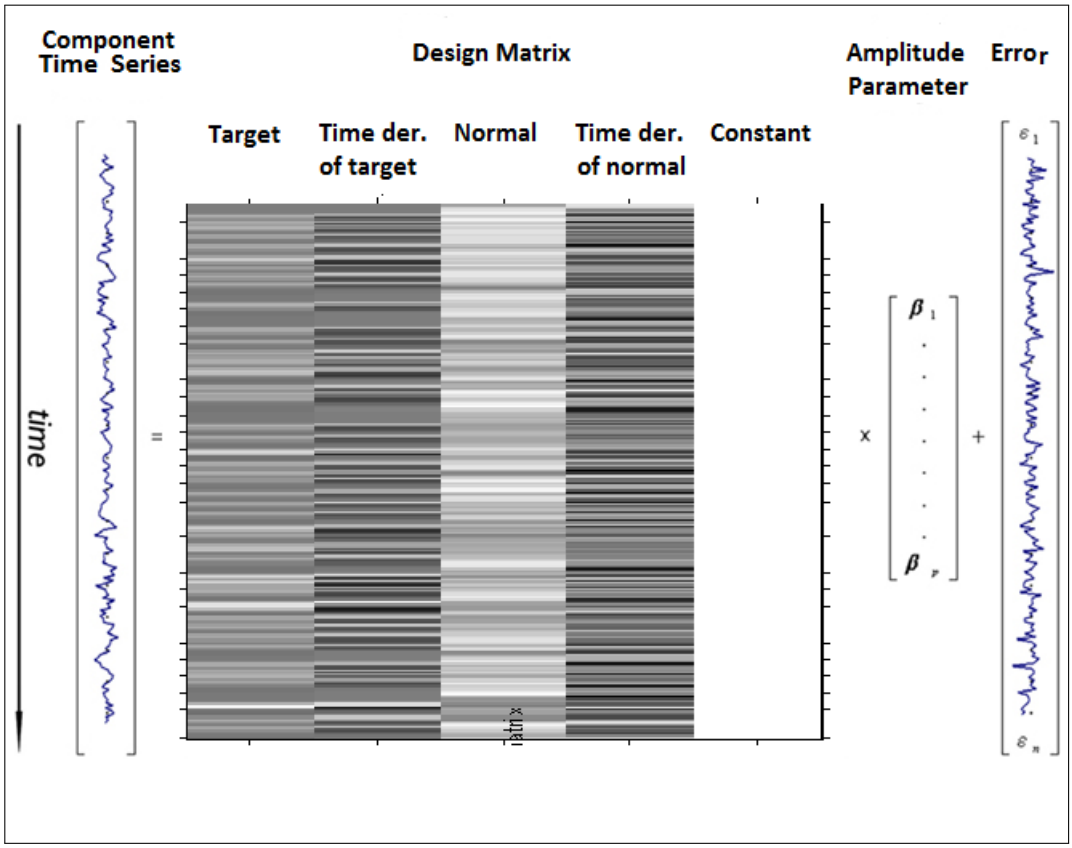

Figure 2.4 Multiple regression for temporal sorting

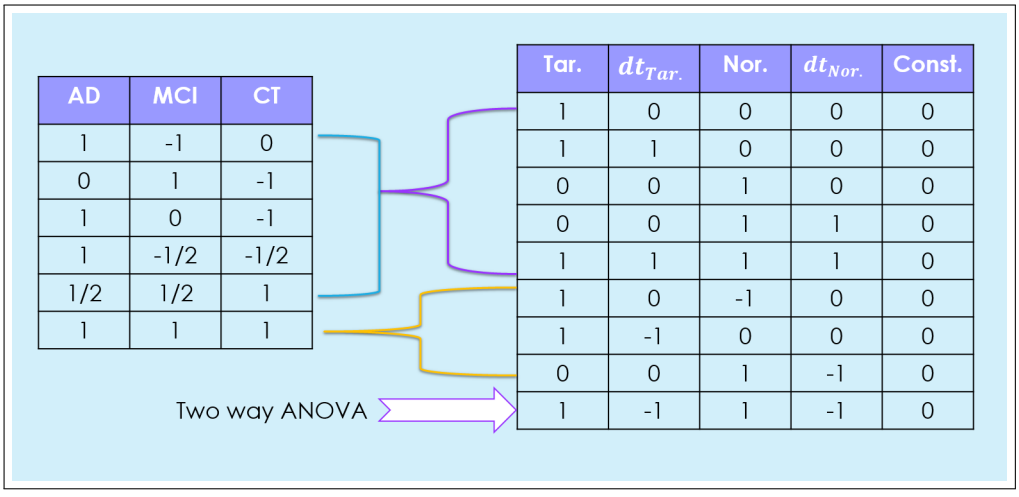

Figure 2.5 Contrasts for the post-hoc, one-way ANOVA statistics on β values can be seen for group comparison as indicated by the combination of blue and purple parenthesis, whereas for regressor comparison as indicated by orange parenthesis. On the other hand, two-way ANOVA contrasts comparing both of the regressors and groups can be seen as the combination of blue parenthesis with the white arrow.

3. RESULTS

The 20, 25, 30, 40, 50, 60 and 75 component results of analyzing subjects all together and separately in groups like AD MCI and CT are viewed by experienced neurologists at Istanbul University Çapa Medical School. The former method with 30 components is thought to give the best network results visually. In order to determine the component number analytically, minimum description length criteria is applied to all of the subjects. The results of MDL criteria can be seen in Figure 3.1 as suggesting 25 components for the analysis. After these steps, the networks are determined via visual inspection with respect to the literature.

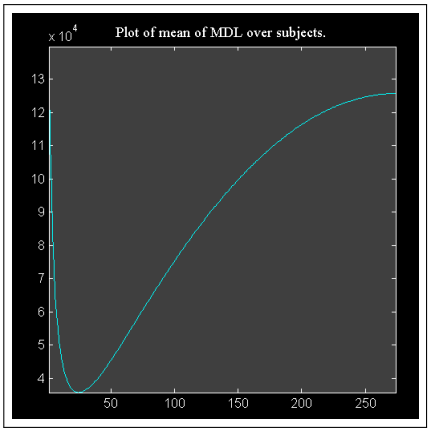

MDL Results for 16 Subjects	
The estimated ICs	25
The mean	24.875
The standard deviation	4.3951
The minimum	18
The maximum	34
The median	24

Figure 3.1 Mean of MDL for 16 Subjects

The results of 30 component ICA, as chosen by the neurologists can be seen in the following sections. When the spectrum analysis of the time courses of components and functional connectivity results after ICA are considered, DARTEL method (Subsection 2.2.3) is found to provide better preprocessing. Thus, only the outcomes of the data preprocessed by DARTEL is used for this chapter.

3.1 ICASSO Results

In Figure 3.2, the stability indexes and total component numbers in each cluster after ICASSO is depicted. Concomitantly, Figure 3.3 show the similarity graph, de-

scribing the clusters. As can be seen from the figures, some of the components are less stable than the others since they have larger extent of red area with total component number under or above 30. In order to choose the most stable estimates among the stochastic results of ICA, the centrotypes, shown as the green circles in the clusters, are chosen. Consequently, these graphs establish the fact that ICASSO is a valuable step for ICA.

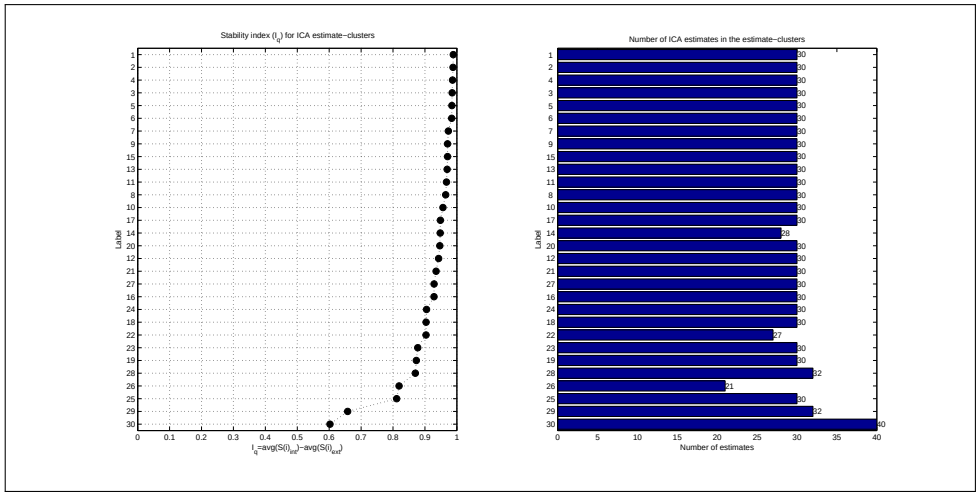

Figure 3.2 Stability Index for DARTEL Method

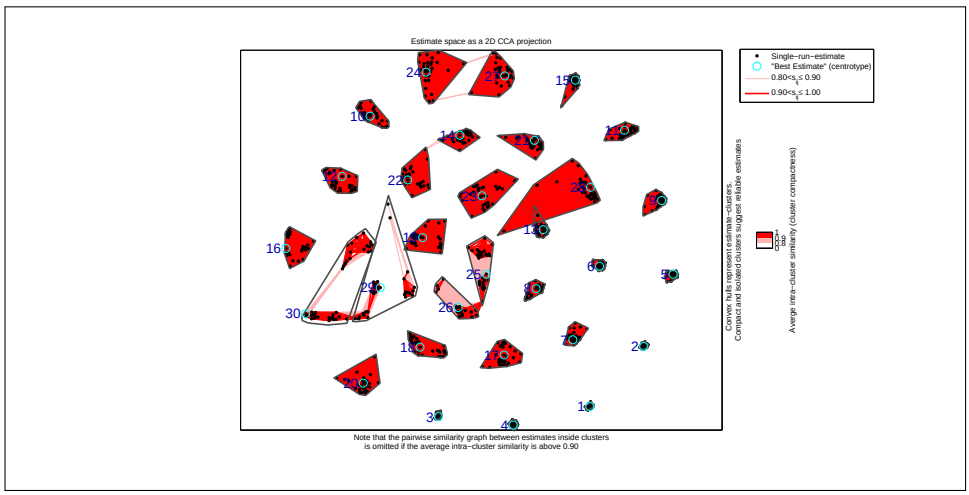

Figure 3.3 Similarity Graph for DARTEL Method

3.2 Attentional Networks

Attentional networks can be divided in subgroups, such as dorsal attention, ventral attention (aggregate of salience and cingulo-opercular networks) [55, 56] and (left and right lateralized) fronto-parietal networks as well as other specialized parts. The name 'attentional' is used for describing the related networks since the paper of Allen and his colleagues ,'A baseline for the multivariate comparison of resting state networks ' [43], providing the basis of this thesis, used this name for a similar group. In some studies [57, 58, 55], the group is named as task positive networks together with sensory mechanism related networks and defined as goal-directed task activated networks [59]. Although those networks are studied and grouped as task-active, they can also be found during resting state [60, 57].

In this analysis 3 different attention related networks are found. Even though it is very common to find dorsal attention and salience networks, there are no networks similar to them among the networks below.

3.2.1 Attentional Network 1

3.2.1.1 Group-wise (All Subjects' Average) Results. In Figure 3.4, midbrain, thalamus and insula are seen as the main parts of the network. There are also other minor brain parts including supplementary motor area. The functional correspondence of these areas are:

Functions of Midbrain (Mesencephalon): Midbrain provides important connections between the constituents of the motor system, such as cerebellum, basal ganglia and cerebral hemispheres. The colliculi constituting midbrain are also involved in auditory and visual reflexes [1]. Those kinds of stimuli are relayed to thalamus from here [61]. Moreover, extraocular muscles controlling the eye movements have cranial nerves directed from this part [1]. It is also thought to be of importance in reward mechanisms and mood [61].

Functions of Thalamus: As the biggest component of the diencephalon, thalamus comprises numerous nuclei, having connections with associative and limbic areas of the cortex, receiving input from the cerebellum and basal ganglia and extending to the motor regions of the frontal lobe, and transmitting general and special sensory information to related parts of the sensory cortices [62]. Sensory information except olfactory is also filtered here [1] .

Functions of Insula: The insula as a hidden part of the cortex under frontal and temporal lobes, has connections with some afferent signal transferring sensory thalamic nuclei. It has (mostly reciprocally) connections with the amygdala as well as with many limbic and association cortical areas [63]. As a result of these connections, it has vast amount of functions. It is one of the pain centers of cortex [62]. It also aids in the involuntary activities like autonomous control of the viscera. There are also extensions of specialized ares in taste and smell sensations [62]. It has shown that the insular cortex has a key role in several auditory processes, such as tuning into novel auditory stimuli and allocating auditory attention. It also has vestibular and somatosensory functions as well as a role in temperature sensation, viscerosensation, somatomotor control, motor plasticity, speech production, cognitive control, bodily awareness, self recognition, individual emotions, social emotions and addiction [63].

Functions of Supplementary Motor Area: Responding to internal cues, specifically intentions to move voluntarily (whether the movement carried out does not matter), is supplementary motor area function [62]. Principally, it arranges the sequences of movements already built in motor memory [62]. Moreover, as an executive control area, initiation of a new action, inhibiting a response plan or flexibly changing the plans as well as sorting out the irrelevant distractors are activation reasons [64].

In the case of this network's activation by the experiment task, the combination of appropriate functions would be about planning the movement necessitated by the oddball task as well as differentiating the normal and target sounds and pressing the button when the target sounds are heard.

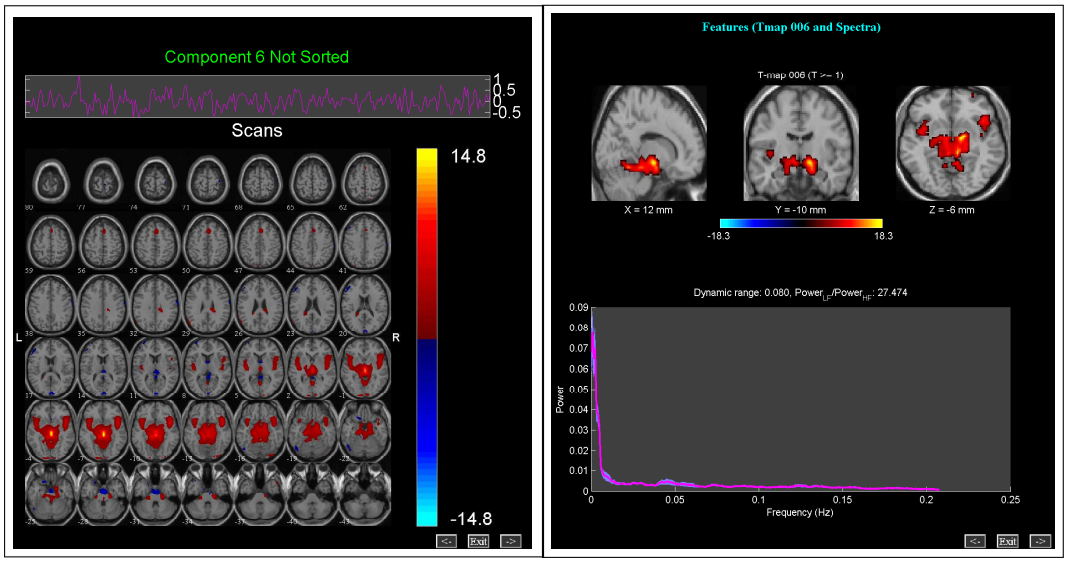

Figure 3.4 Attentional Network 1

3.2.1.2 Subject-wise results. When the statistics on β values are considered, the results for targets regressor are found to be greater for AD and CT than MCI with $p \leq 0.02$.

3.2.2 Attentional Network 2

3.2.2.1 Group-wise Results. In Figure 3.5, the main functional divisions are frontal lobe, temporal lobe, inferior parietal lobule, anterior cingulate, and precuneus. As can be seen, mostly the right part of the brain is active. This network is called right lateralized fronto-parietal network or fronto-parietal control network or multiple demand system [60, 43, 12, 65, 58] in structure-wise nomenclature and right executive network [66, 57] in functional nomenclature. However, in some studies like in Smith and his colleagues', executive network is described as consisting of several medial-frontal areas (including anterior cingulate and paracingulate) apart from the fronto-parietal control network consistent with the one in Figure 3.5 [67].

This network has shown to be involved in various cognitive processes, such as reasoning, attention, inhibition, memory (working memory, episodic memory) and mental imagery [60, 58]. Moreover, the adaptability in implementation of various tasks

are thought to be provided via this network as its parts act like flexible hubs [68]. Which means that the parts of this networks adapt their pattern of global functional connectivity according to the tasks. It is also shown that the relation between the DMN and the dorsal attention network is moderated by this network as an intrinsic control mechanism [57, 58]. Thus, in this study it might work as the intrinsic control mechanism, attention and inhibition processor.

If all of the regressors are considered for sorting the components according to their task relatedness, this component has the 3rd place. Apart from that, there are no other significant results.

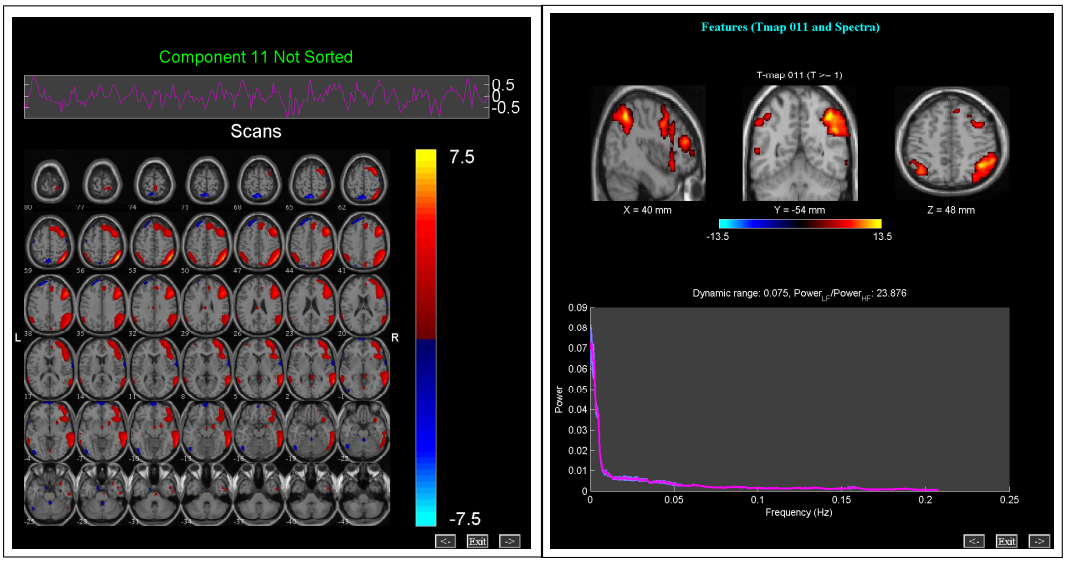

Figure 3.5 Attentional Network2

3.2.3 Attentional Network 3

3.2.3.1 Group-wise Results. As can be seen from Figure 3.6, the network mainly consists of parietal lobe and precuneus which is in the medial posterior parietal cortex. A similar network is found in Allen and his colleagues' study [43] (as IC 72), with the function of directing attention among the attentional networks group. In order to look closely to this component, the largest and the most active part in the network can be examined as well as its connections with the other parts in the network. Moreover, the connections of this network with others are of importance. Below is the main part of

this network, precuneus:

Precuneus: It has three functionally discrete regions, namely the dorsal-anterior precuneus connected with medial somatomotor regions, the posterior precuneus connected with visual areas, and the ventral precuneus connected with the dorsolateral prefrontal cortex, the inferior parietal lobule, and the superior temporal sulcus [69, 70]. Functionally, precuneus is involved in reflective, self-related processing, awareness and conscious information processing, episodic memory, and visuospatial processing [70]. Generally, it becomes more active during rest than a task [70]. Moreover, connectivity patterns are dynamic, like connectivity between the precuneus and the right frontoparietal network increases during task whereas connectivity between the precuneus and the default-mode network (DMN) during rest [71]. As the effect is greater for the rest state, it is thought to be more specialized towards cognition during resting state [71]. If the task is autobiographic rather than externally stimulating, precuneus becomes a part of DMN [65].

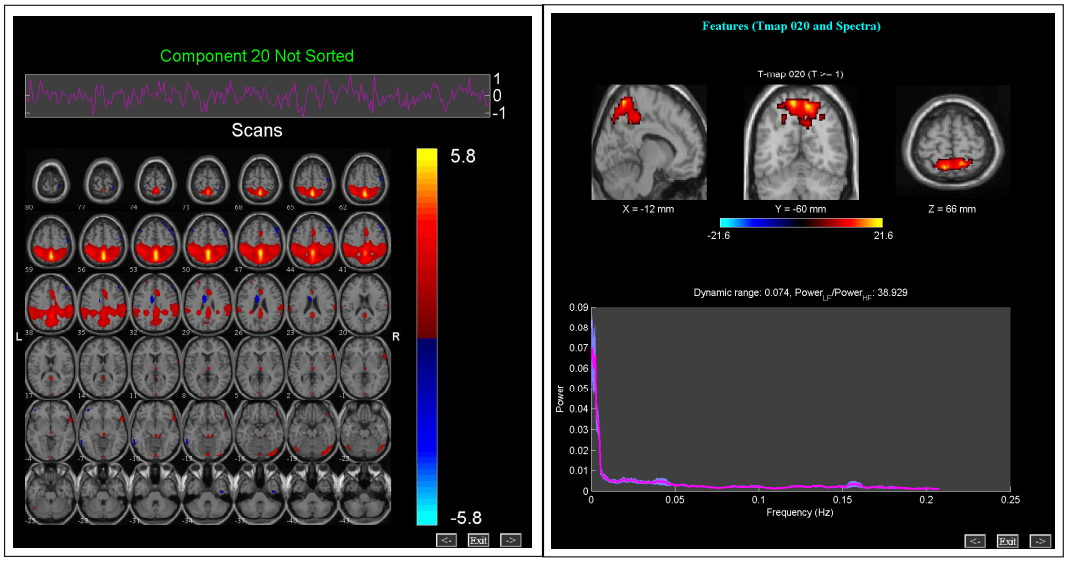

Figure 3.6 Attentional Network 3

In Figure 3.7, functional connectivity map of this study can be seen. There are 30×30 squares, representing the correlation of 30 components with each other. The color of each square depicts the value of z-score obtained by the transformation

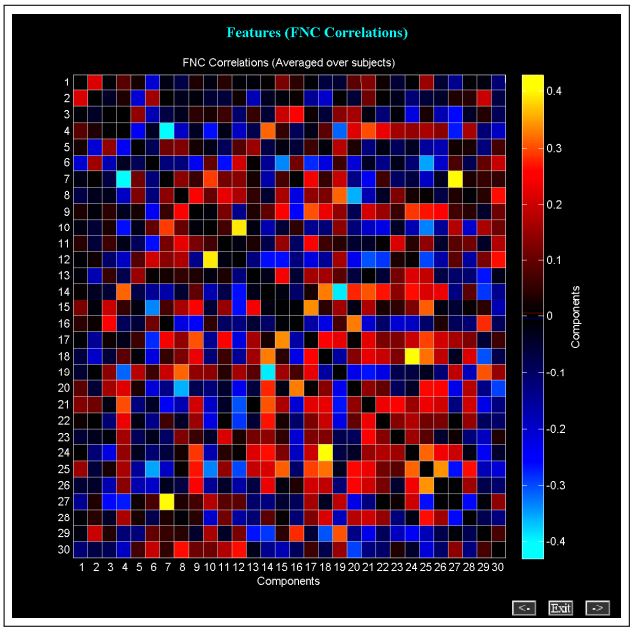

Figure 3.7 Functional network connectivity

of the correlation coefficient of the two components. According to that map, this component have both positive and negative correlation with DMN as shown in the Figure 3.8. Negative correlation is thought to reflect the inverse working mechanism of the components, such as one is active whereas the other is inactive. Consequently, the positive correlation means that the networks become activated together.

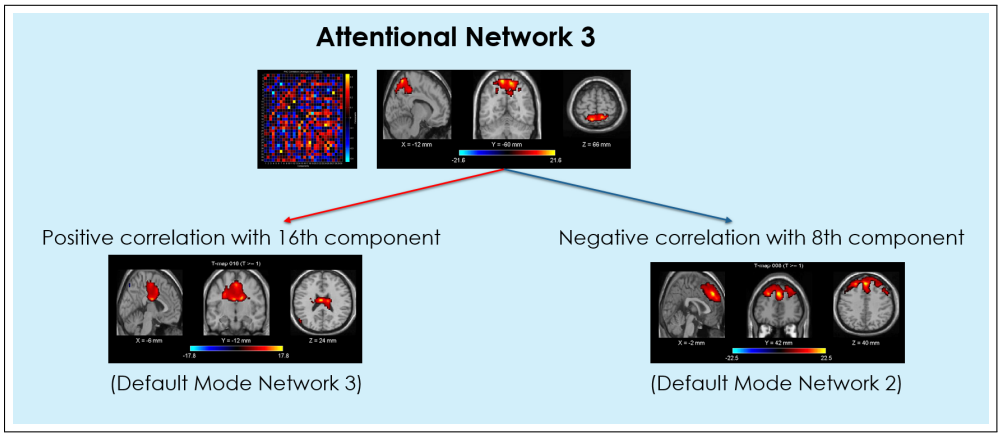

Figure 3.8 Functional network connectivity of attentional network 3

3.2.3.2 Subject-wise Results. This component has both the spatial map difference among AD and MCI ($p < 0.05$) and β value variation. The spatial map variation

does not exceed 5 voxel in the precuneus area (Figure 3.9). As for the statistics of β values:

- **For all of the regressors:** With a contrast of $MCI > AD$ (meaning a contrast of $[-110]$ for a group like AD, MCI and CT), p value is found to be 0.02, indicating a significant difference.
- **For normals and time derivative of normals:** For the contrasts $CT > AD$ and $MCI > AD$, the p values are found to be 0.03 and 0.0007 subsequently.
- **For normals:** With the contrast of $MCI > AD$, $p = 0.003$.
- **For targets:** With the contrast of $MCI > AD$, $p = 0.05$.
- **Two way ANOVA:** With the contrast $MCI > CT$ & $Targets > Normals$, p=0.002.

Thus, it might be said that this network first becomes enhanced and as the disease progresses, it becomes disrupted.

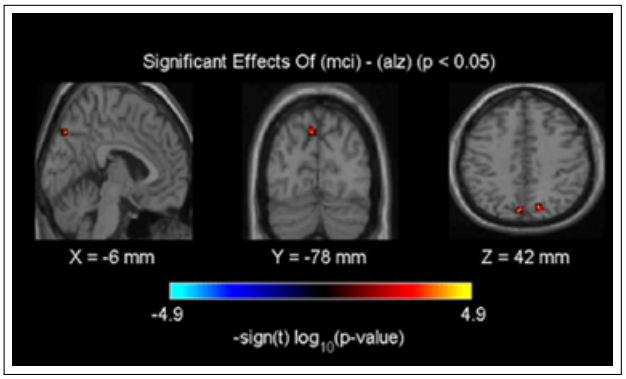

Figure 3.9 Spatial map difference of attentional network 3 between AD and MCI

3.3 Auditory Network

3.3.1 Group-wise Results

In Figure 3.10, as the most prominent parts are the superior temporal, insular and postcentral cortex, it can be seen that the network is auditory network consistent with the literature [43, 72, 73, 74]. As the name suggests, this network is involved in audition including tone/pitch discrimination, oddball discrimination, phonological discrimination, music and speech (in paradigms like action-execution-speech, cognition-language-speech) [67, 60, 74].

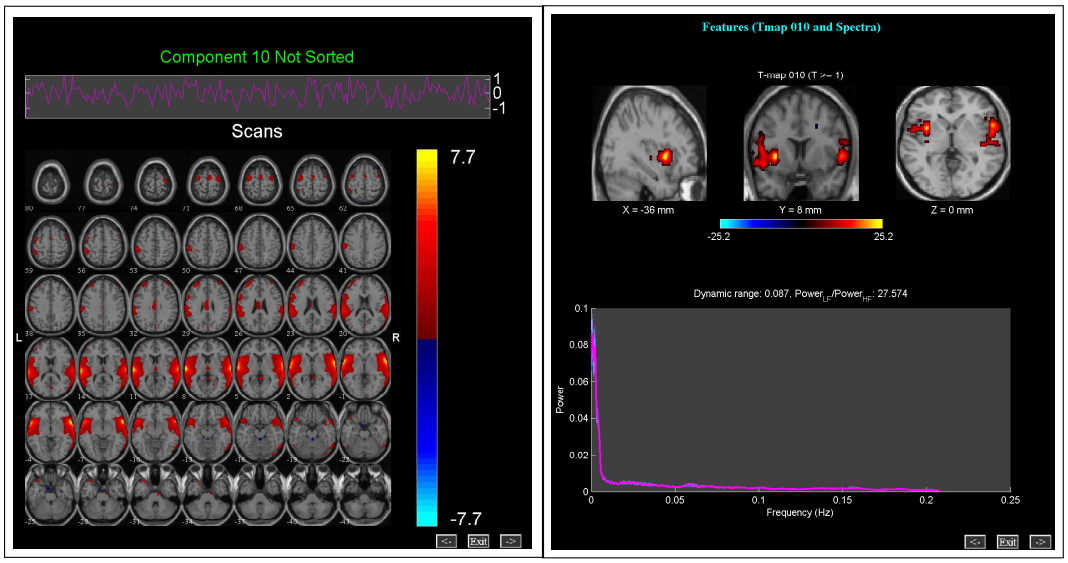

Figure 3.10 Auditory Network

3.3.2 Subject-wise Results

The outcomes are significant only for the β value statistics. The contrasts having prominent results are $AD > CT$ & $Targets > Normals$ and $MCI > CT$ & $Targets > Normals$ with $p = 0.02$ and $p = 0.0046$.

3.4 Cerebellum

3.4.1 Group-wise Results

In Figure 3.11, the most prominent part is cerebellum. There are similar networks found in literature, and declared to be involved in action-execution and perception-somesthesis-pain chains as well as a variety of sensorimotor, autonomic and cognitive functions [67, 60, 74].

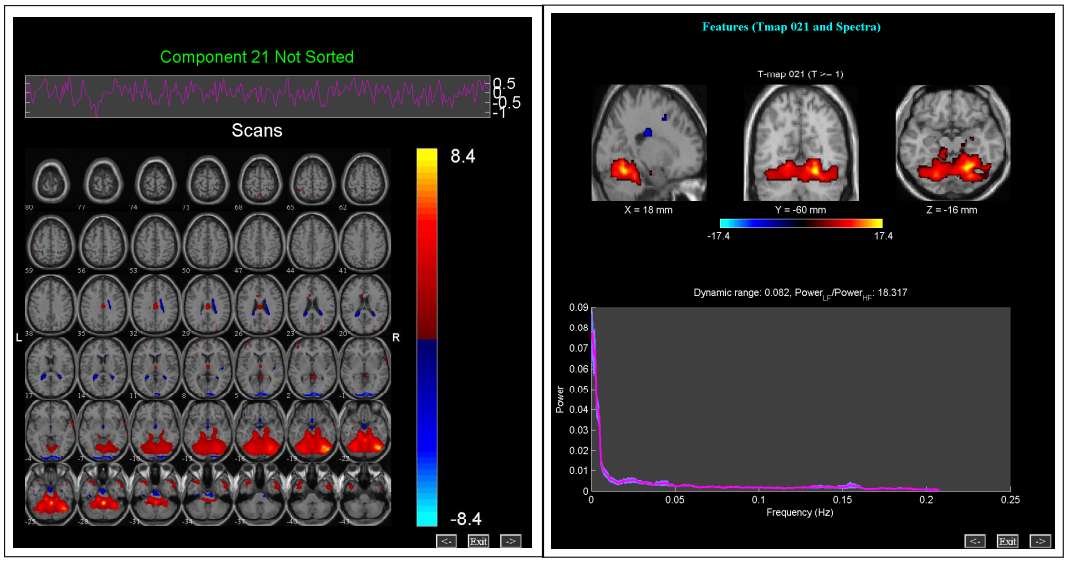

Figure 3.11 Cerebellum

3.4.2 Subject-wise Results

The significant differences are only found for the β value statistics. They can be summarized as:

- **For all of the regressors:** With a contrast of $MCI > AD$, p value is found to be 0.04, indicating a significant difference.
- **For normals and targets:** For the contrasts $CT > AD$ and $CT > MCI$ the p values are found to be 0.01 and 0.03 subsequently.

- **For targets and time derivative of targets:** With the contrasts of $CT > AD$ and $MCI > AD$, p values are 0.03 and 0.003 respectively.
- **For targets:** With the contrasts of $CT > AD$ and $CT > MCI$, p values are 0.002 and 0.008 respectively.

The values seem higher for the healthy elderly and lower for the AD patients.

3.5 Default Mode Network (DMN)

The default mode network is one of the most studied networks for connectivity patterns indicating pathological markers (especially for autism, schizophrenia, and Alzheimer's disease). It is consisted of medial prefrontal cortex, posterior cingulate cortex, superior and inferior frontal gyri, medial and lateral temporal lobes and the posterior extent of the inferior parietal lobule [65]. Those regions are also thought to be anatomically connected directly or indirectly apart from their intrinsic functional connectivity [75]. As do the most of the components, the default mode network is also present whether there is a task. It is mostly active during rest, internal mentation and mind wandering (both in undirected cognition state and sustained attention states) [75, 76]. However, it becomes deactivated when the task positive networks are active. These networks are anti-correlated moment to moment even in the absence of a task. Thus, it is thought that this anti-correlation may act as an unwanted thought inhibitor [57]. As a control mechanism on being activated and deactivated, salience network is thought to play an important role by activating executive network while deactivating DMN. Moreover, in mediating the the relations between dorsal attention network, fronto-parietal network is found to be involved [57].

Apart from the functional and structural properties, this network is thought to be involved in progression of AD. The disruption of the network activity, especially decrease in task induced deactivation and disruption of molecular cascades in exactly the same regions corresponding to DMN leads to a probability of a conclusion that

it might indeed be a cause rather than a consequence [57, 10]. Thus, this network's activity might accelerate the process of the AD pathology [57].

In this study, 5 networks related to DMN, consistent with the literature are found.

3.5.1 DMN 1

3.5.1.1 Group-wise results. As can be seen from Figure 3.12, the most prominent parts of this network are medial frontal gyrus and cingulum.

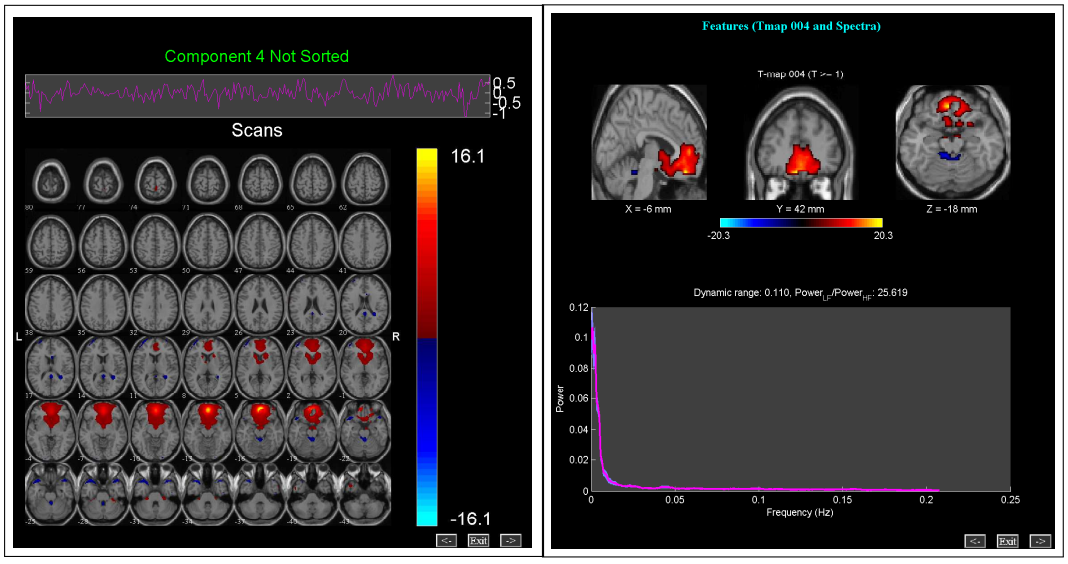

Figure 3.12 DMN 1

In Figure 3.13, the functional connectivity of this network is depicted as positive with the 3rd visual network whereas negative with the 1st visual network.

3.5.1.2 Subject-wise results.

- **For normals:** With the contrasts $CT > AD$ and $CT > MCI$, $p = 0.04$ and $p = 0.02$ respectively.

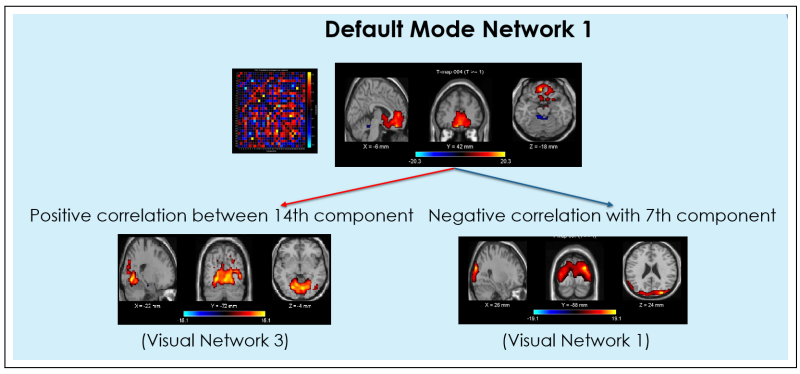

Figure 3.13 Functional connectivity of DMN 1

- **For targets and time derivative of targets:** With the contrast $MCI > AD$, $p = 0.058$.
- **Two way ANOVA:** With the contrasts $AD > CT$ & $Targets > Normals$, $AD > MCI$ & $Targets > Normals$, and $MCI > CT$ & $Targets > Normals$, $p = 0.005$, $p = 0.0047$, and $p = 0.05$ with negative t values respectively.

3.5.2 DMN 2

3.5.2.1 Group-wise results. As can be seen from Figure 3.14, the most prominent parts of this network are superior frontal gyrus and medial frontal gyrus.

In Figure 3.15, functional connectivity of this network with the 3rd attentional network is depicted as negative.

3.5.2.2 Subject-wise results. The significant results of statistical analysis of β values are:

- **For normals and time derivative of normals:** With the contrast AD>MCI, $p = 0.02$.

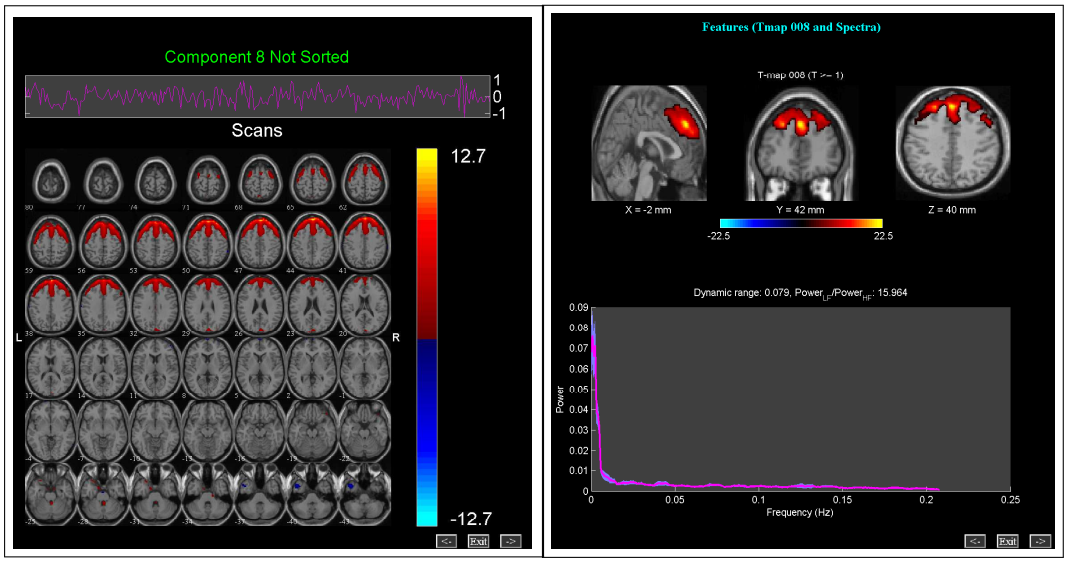

Figure 3.14 DMN 2

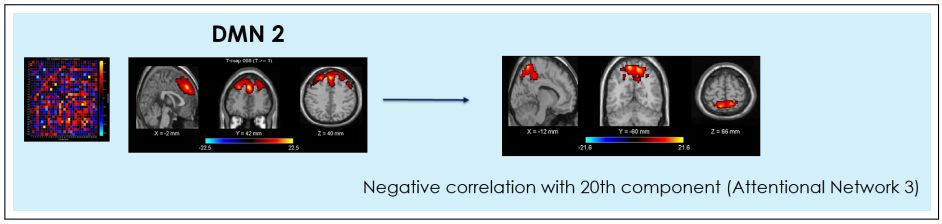

Figure 3.15 Functional connectivity of DMN 2.

- **For normals:** With the contrasts $AD > CT$ and $AD > MCI$, $p = 0.05$ and $p = 0.009$ respectively.

3.5.3 DMN 3

3.5.3.1 Group-wise results. As can be seen from Figure 3.16, the most prominent part of this network is limbic lobe. Moreover, positive correlation with the 3rd attentional network is observed (Figure 3.17).

3.5.3.2 Subject-wise results. As can be seen in Figure 3.18, the difference in spatial maps of controls and AD patients is located in white matter of sub-gyral frontal lobe. The voxel count in the area does not exceed 5.

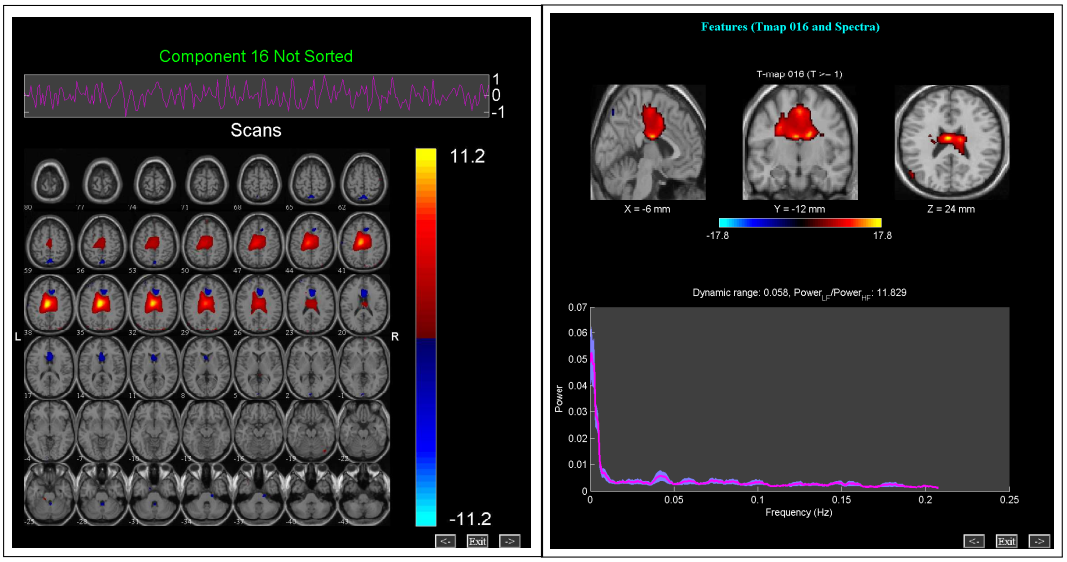

Figure 3.16 DMN 3

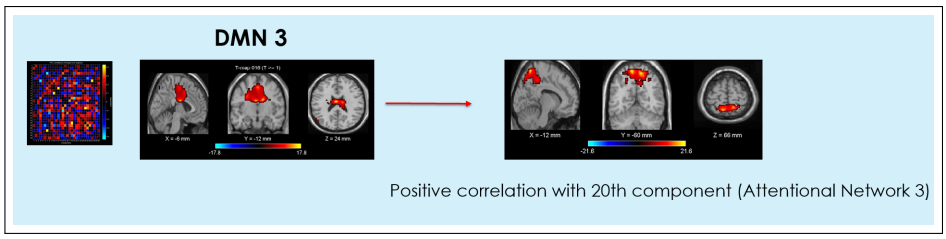

Figure 3.17 Functional connectivity of DMN 3

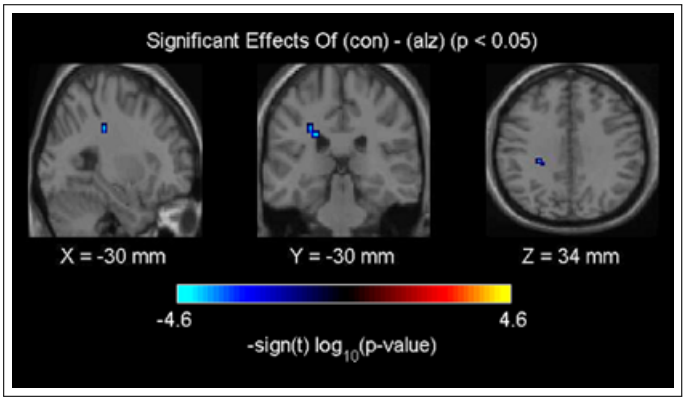

Figure 3.18 Spatial map difference of DMN 3 between controls and AD patients

3.5.4 DMN 4

3.5.4.1 Group-wise results. As can be seen from Figure 3.19, the most prominent part of this network is medial frontal gyrus.

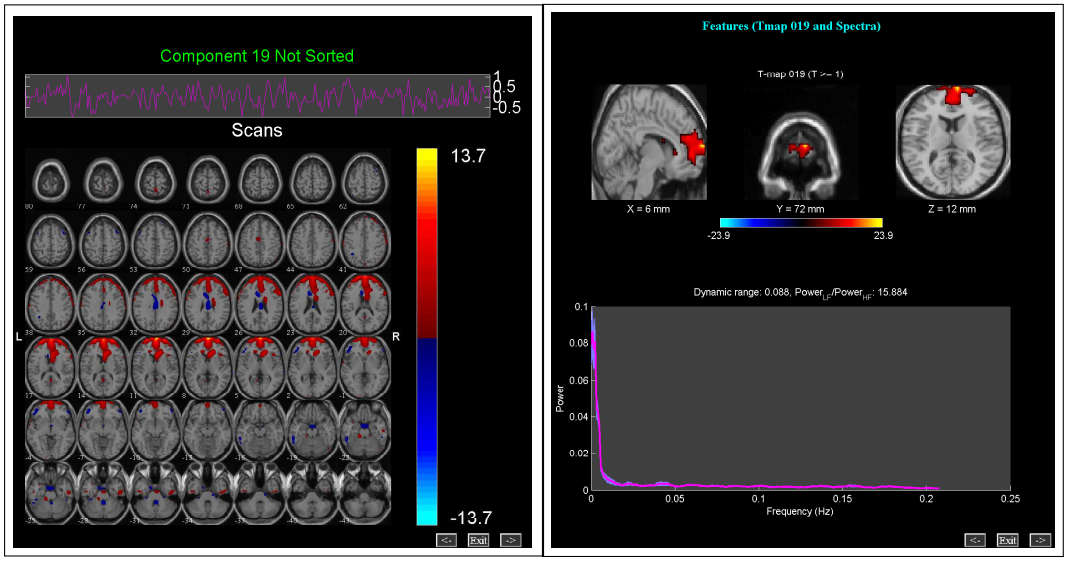

Figure 3.19 DMN 4

In Figure 3.5.4.1, the functional connectivity of this network with the 3rd Visual Network is depicted as negative.

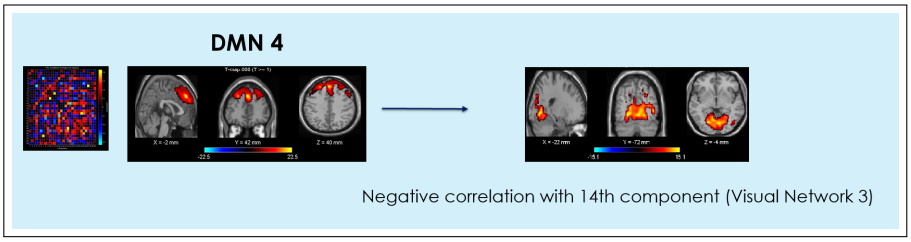

Figure 3.20 Functional Connectivity of DMN 4

3.5.4.2 Subject-wise results. Significant differences are found for the β values as:

- **For all regressors:** With the contrast $MCI > AD$, $p = 0.05$.

- **For normals and time derivative of normals:** With the contrasts $CT > AD$, and $MCI > AD$, $p = 0.03$ and $p = 0.03$ respectively.
- **For normals:** With the contrasts $CT > AD$, and $MCI > AD$, $p = 0.03$ and $p = 0.03$ respectively.

3.5.5 DMN 5

3.5.5.1 Group-wise results. As can be seen from Figure 3.21, the main parts of this network are temporal lobe, precuneus, posterior cingulate and medial frontal gyrus. The most common pattern of DMN matches very well with this network. However, there are no other outcomes related with the subjects.

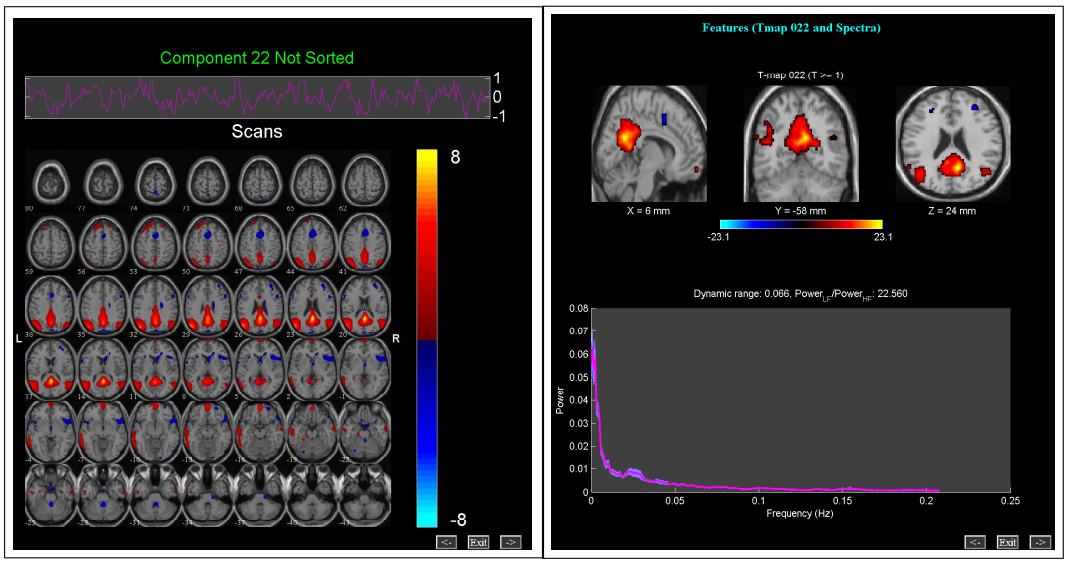

Figure 3.21 DMN 5

3.6 Frontal Network

3.6.1 Group-wise results

In figure 3.22, one network which can be named as frontal network [43] is present. The most prominent parts are inferior and middle frontal gyrus along with the pre-

central gyrus. Those areas are known to aid in motor control, executive, memory and language related functions [43, 77].

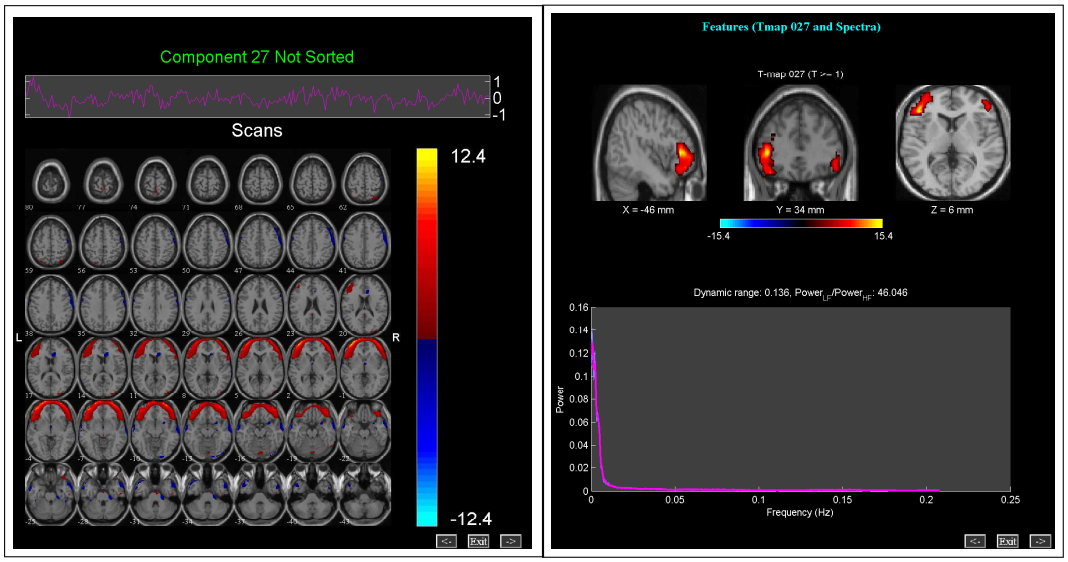

Figure 3.22 Frontal Network

In Figure 3.23, the functional connectivity of this network with the 1st visual network is depicted as positive.

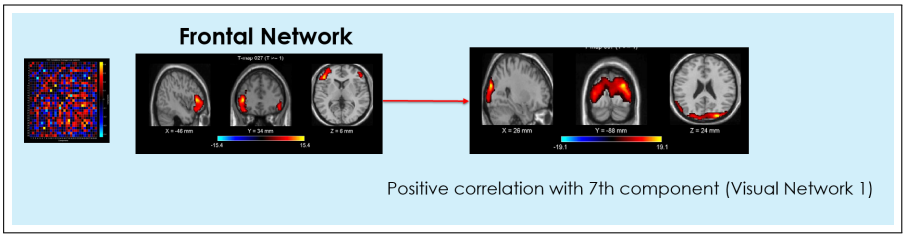

Figure 3.23 Functional connectivity of frontal network

3.7 Sensorimotor Network

3.7.1 Group-wise results

In figure 3.24, the most prominent parts are precentral and postcentral gyruses. Thus, it can be named as sensorimotor network as in the literature [67, 43]. It is the first network to be found for resting state fMRI data. Action-execution and perception-somesthesis paradigms specifically involving hand movements are shown to activate this network [67, 60].

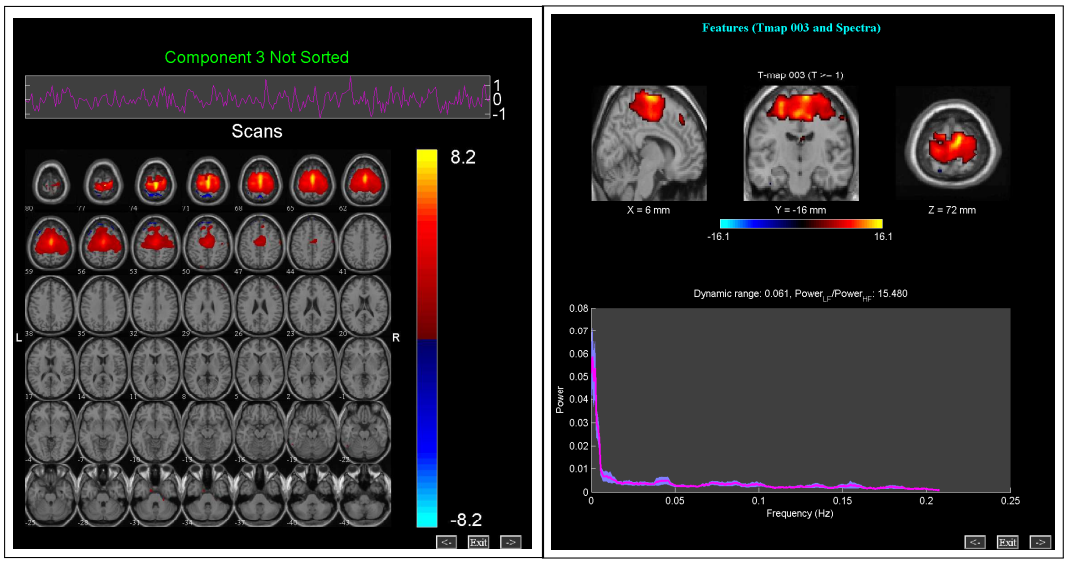

Figure 3.24 Sensorimotor Network

3.7.2 Group-wise results

The significant results of the statistical analysis of β values can be summarized as:

- **Two way ANOVA:** With the contrasts $AD > CT$ & $Targets > Normals$ and $MCI > CT$ & $Targets > Normals$, $p = 0.058$ and $p = 0.009$ respectively.

3.8 Visual Network

This network can be divided into subgroups as medial occipital pole and lateral visual areas. These sub-networks are known to be involved in functions for paradigms cognition-language-orthography and covert reading and cognition-space (like mental rotation and location discrimination in space) [67, 43, 60]. Moreover, functions related to viewing such as visual stimuli involving emotional content, action observation, moving object tracking, overt picture naming concerns this area [60]. As for a demonstration of plasticity of the brain, Braille reading is found to activate these networks [60]. Additionally, the functional connectivity of these areas are found to be dynamic in nature. It becomes connected with fronto-parietal network when task related relevant visual information is processed whereas with DMN if irrelevant visual information is processed [78].

In this study, there are 4 networks related to this group.

3.8.1 Visual Network 1

3.8.1.1 Group-wise results. As can be seen from the Figure 3.25, the network includes inferior temporal gyrus, middle temporal gyrus, occipital lobe (mostly middle occipital gyrus and superior occipital gyrus with BA 19 and 18 - secondary, and tertiary visual cortices).

In Figure 3.26, Functional connectivity of this network is depicted as positive with the frontal network whereas negative with the 1st DMN.

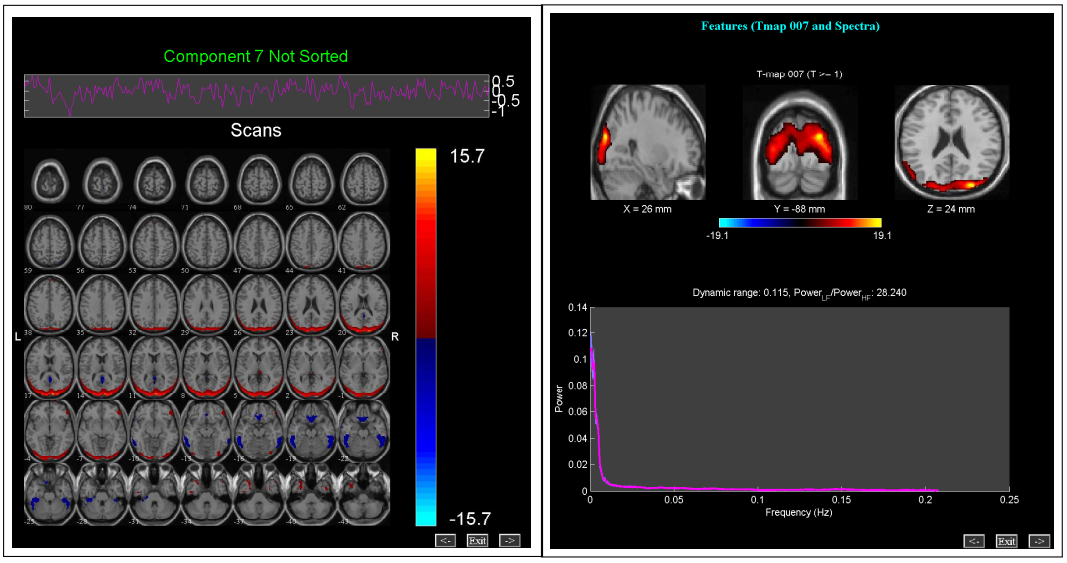

Figure 3.25 Visual Network 1

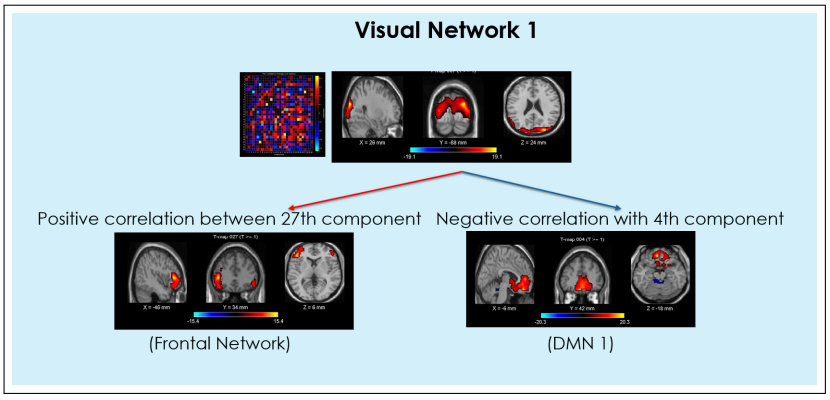

Figure 3.26 Functional connectivity of visual network 1

3.8.2 Visual Network 2

As can be seen in figure , the most prominent parts are middle occipital gyrus, middle temporal gyrus, lingual gyrus, inferior temporal gyrus, fusiform gyrus with some limbic sytem elements as well as related cerebellum, frontal and parietal lobe parts.

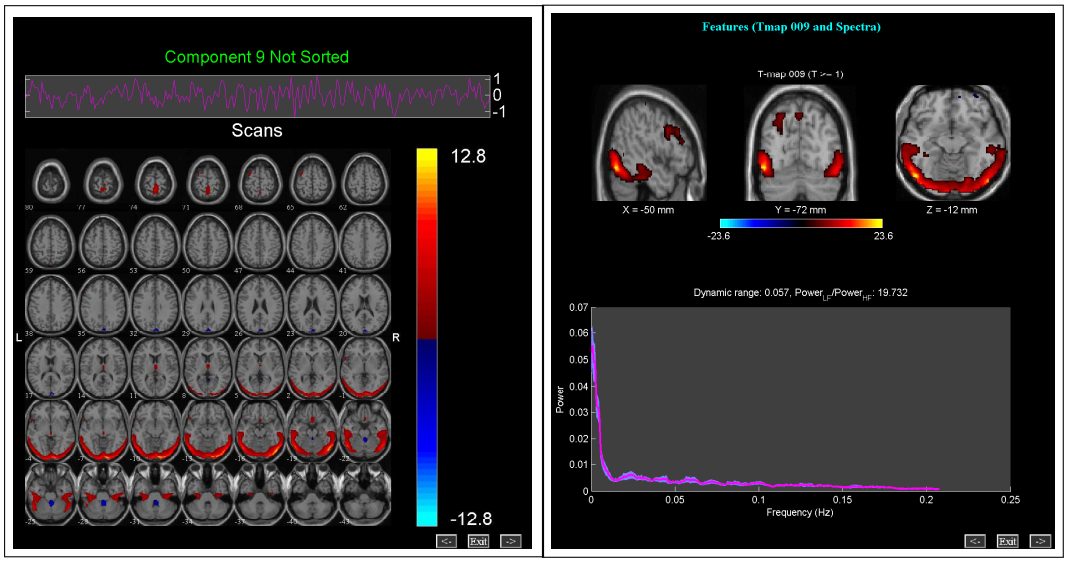

Figure 3.27 Visual Network 2

3.8.3 Visual Network 3

3.8.3.1 Group-wise results. As can be seen from the Figure 3.28, the most prominent parts are occipital lobe, limbic lobe and supplementary motor area.

In Figure 3.29, the functional connectivity of this network is depicted as positive with the 1st DMN whereas negative with the 4th DMN.

3.8.3.2 Subject-wise results. The most prominent results of the statistical analysis of the β values can be summarized as:

- **For normals and targets:** With the contrast $AD > MCI$, $p = 0.03$.

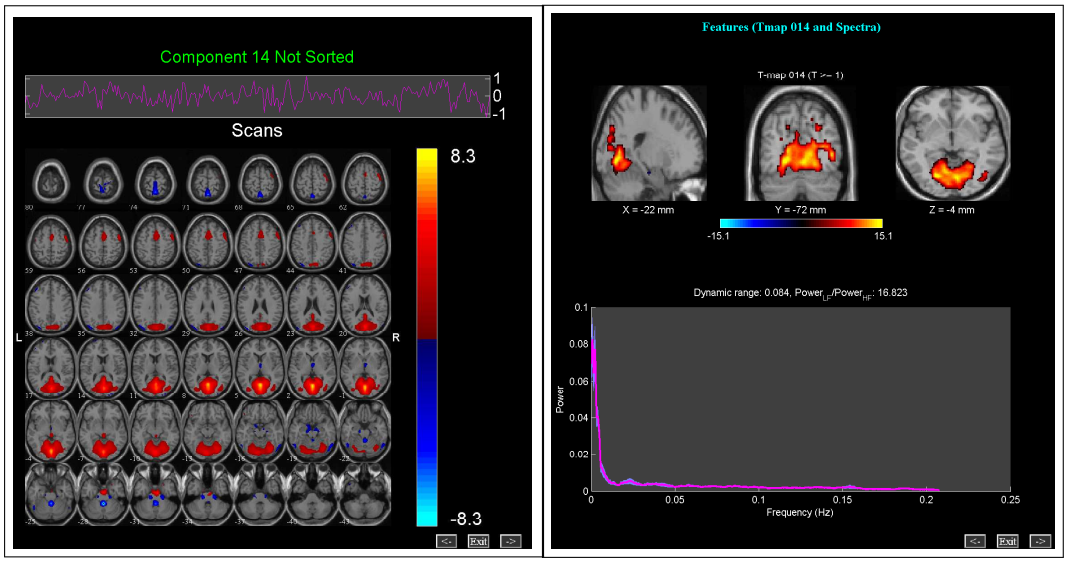

Figure 3.28 Visual Network 3

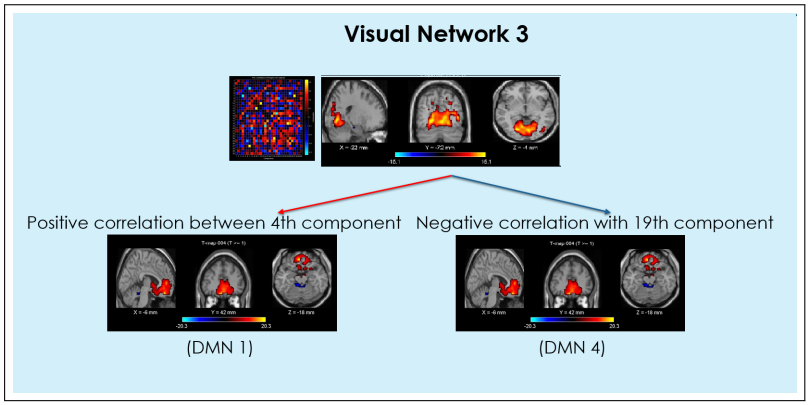

Figure 3.29 Functional connectivity of visual network 3

- **For targets:** With the contrasts $AD > CT$, and $AD > MCI$, $p = 0.03$ and $p = 0.004$ respectively.

3.8.4 Visual Network 4

3.8.4.1 Group-wise results. As can be seen from the figure , the most prominent parts are precuneus, occipital lobe, fusiform gyrus, middle temporal gyrus, thalamus and certain parts of parietal lobe.

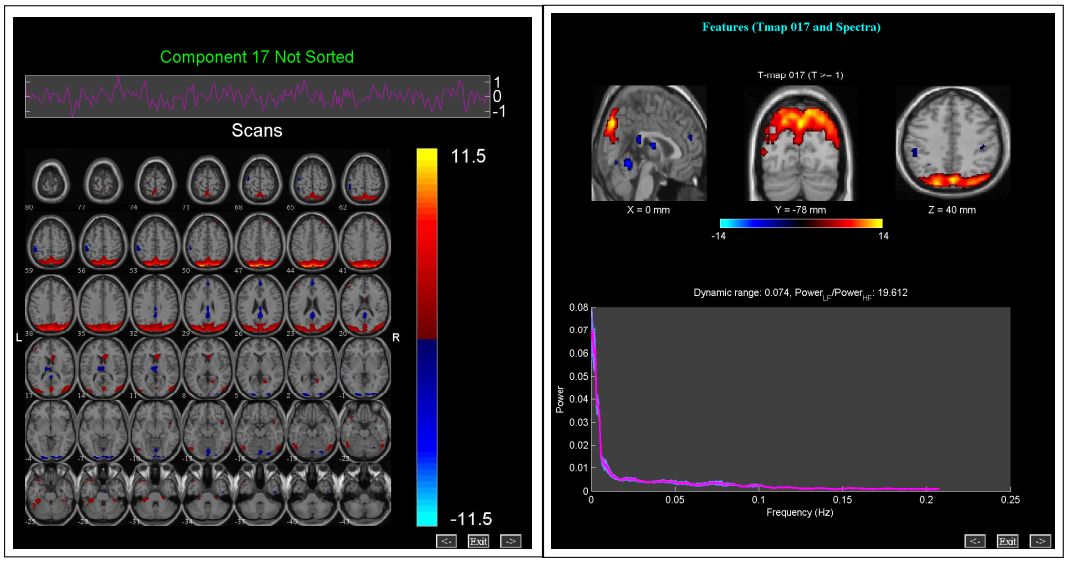

Figure 3.30 Visual Network 4

3.8.4.2 Subject-wise results. The significant results of the statistical analysis of the β values can be summarized as:

- **For all regressors:** With the contrast $CT > AD$, $p = 0.03$.
- **Two way ANOVA:** With the contrast $AD > CT$ & $Targets > Normals$, $p = 0.01$ with a negative t value.

3.9 Unclassified Network

3.9.1 Group-wise results

As can be seen in Figures 3.31 and 3.32, the main parts of this network are temporal lobe (mostly left middle temporal gyrus, superior temporal gyrus), inferior and superior frontal gyrus and supramarginal gyrus. In the literature, there is not a network resembling exactly to this network. That may be also due to the clinical fMRI data having some of the temporal slices lost due to the FOV and the very old population used as subjects. However, partial overlapping with three different networks is detected. Those networks include ventral stream [72, 73, 79], semantic network, auditory processing network [80, 81] and temporo-parietal network [82]. The sagital view of the network, which can give a better presentation of the activation locations in this case, can be seen in Figure 3.31. Below are the functions of the most pronounced areas as well as their connections with each other:

Middle temporal gyrus It aids in language comprehension (lexical syntactic information retrieval, resolution of ambiguity) [83], multimodal semantic processing (verbal and non-verbal), semantic memory, auditory and visual information integration (information comes laterally from superior temporal gyrus and fusiform gyrus) [81].

Superior temporal gyrus It has functions in auditory processing together with language, reading, verbal semantic processing, social cognition with the interactive pathways between amygdala, prefrontal cortex and other frontotemporolimbic structures, regulation of behavior, and neural mechanisms of imitation [84, 85, 81].

Temporal pole It has 4 major divisions as the dorsal part, with predominant connectivity to auditory, somatosensory and language networks; the ventromedial part, predominantly connected to visual networks; the medial part, connected to paralimbic structures; and lastly the anterolateral part, connected to the default-semantic network. Thus, it has functions in language, semantic and lexical skills,

visual cognition, face recognition, semantic memory, high-level visual and auditory processing (face familiarity judgments, understanding emotion through faces, integrating visual and auditory information in semantic tasks, the analysis of musical melody, the identification of speakers via their voice, face and name association), socio-affective behavior like empathy, regulation of eating and sexual behavior. It is also found that the semantic tasks involving auditory stimuli activates the left temporal pole more robustly [80].

Inferior frontal gyrus It aids in language comprehension (unification via maintenance, selection and integration of various sources of information over time) [83], multimodal semantic processing (more precisely semantic controlling in order to behave as time and context necessitates) [81].

Superior frontal gyrus With the help of diffusion tensor tractography, it is divided into 3 subregions namely anteromedial, dorsolateral and posterior [77]. The anteromedial part is found to be anatomically connected with the anterior and mid-cingulate cortices; thus, aiding in the functions of cognitive control and default mode network. Also, it has strong resting state functional connectivity with the posterior cingulate cortex, caudate, middle frontal gyrus, thalamus, and the opercular and triangular parts of inferior frontal gyrus, which are mostly the parts found in this network (Figure 3.32). The dorsolateral part is found to be anatomically connected with the middle and inferior frontal gyri; thus, aiding in functions of cognitive execution network. In addition, it has some weak resting state functional connectivity with the anterior cingulate cortex, posterior cingulate cortex and caudate nucleus. Lastly, the posterior part is found to be anatomically connected with the precentral gyrus, caudate, thalamus, and frontal operculum; thus, aiding in the functions of motor control network. Additionally, it has a strong resting state functional connectivity with mid-cingulate cortex, sensorimotor and speech relate brain areas [77].

Supramarginal gyrus It is involved in verbal working memory [86], self generated and observed actions [87]. Moreover, the part in the right hemisphere is involved in self-other distinction, overcoming self egocentricity bias [88], accurate perception of being upright via processing information from multiple modalities [89].

As can be seen, most of the divisions are a part of language or semantic processing network especially when they are connected. If looked at the possible networks described above as ventral stream, semantic network, auditory processing network and temporo-parietal network, there are lots of common structures and functions (especially with temporo-parietal network). The exact naming and functional attribution can only be done after a through research.

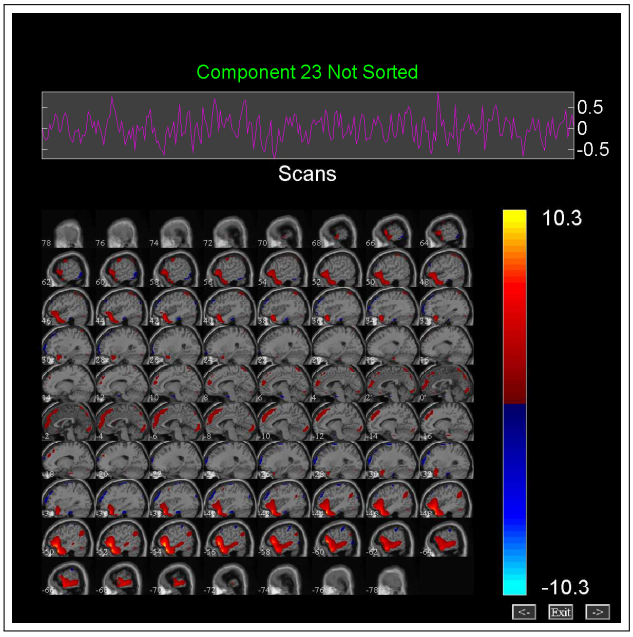

Figure 3.31 Sagital view of 3rd attentional network

3.9.2 Subject-wise results

The significant results of the statistical analysis of the β values can be summarized as follows:

- **For targets and time derivative of targets:** With the contrast $CT > AD$, $p = 0.04$.
- **Two way ANOVA:** With the contrast $AD > CT$ & $Targets > Normals$, $p = 0.02$ with a negative t value.

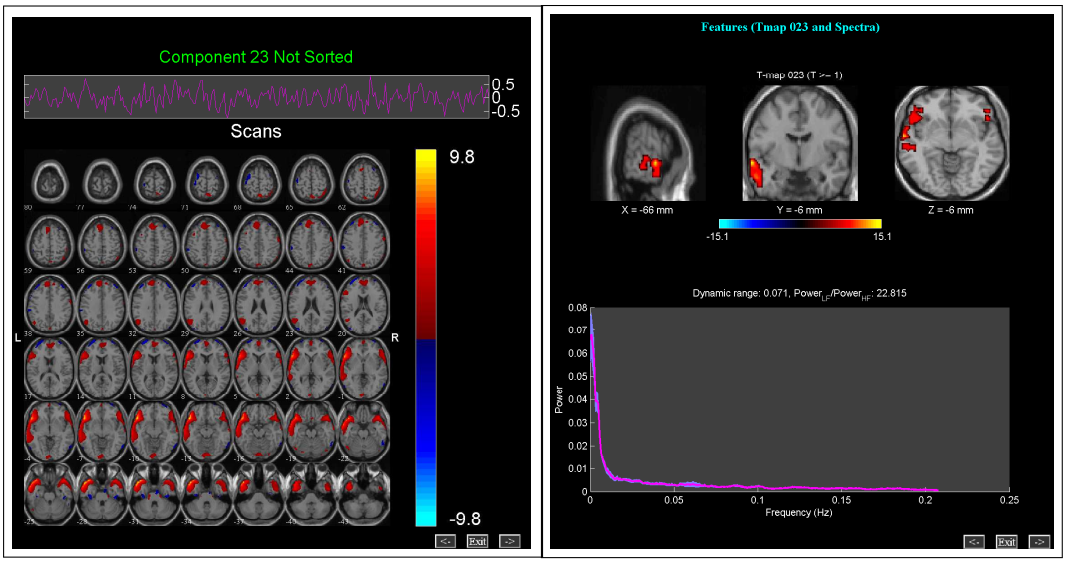

Figure 3.32 Unclassified Network

3.10 Spectral Analysis of Temporal Courses

In Figure 3.33, the dynamic range vs. power ratio graphs can be seen. Those graphs are the results from baseline corrected and despiked temporal courses of components obtained after the preprocessing steps. The colors refers to the network groups explained above and the number labels represent the component numbers. As can be seen from Figure 3.33, the artifacts (red ones) tend to assemble to the left part of the graph. This effect is expected since the literature suggest artifacts mostly have lower dynamic range and power ratios [43] due to their noisy structure. The graph can also be used as a measure to check the visual artifact selection. In addition to to this graph, the spectral graphs under the t-maps in the network subsections might also be used to infer about the artifacts since the artifact spectras tend to have more variation among subjects.

Apart from these results, the method is also applied to detrended and despiked temporal courses. As expected, it does not give awaited results. Therefore, it can be said that detrending badly affects temporal courses of the components of the task related fMRI.

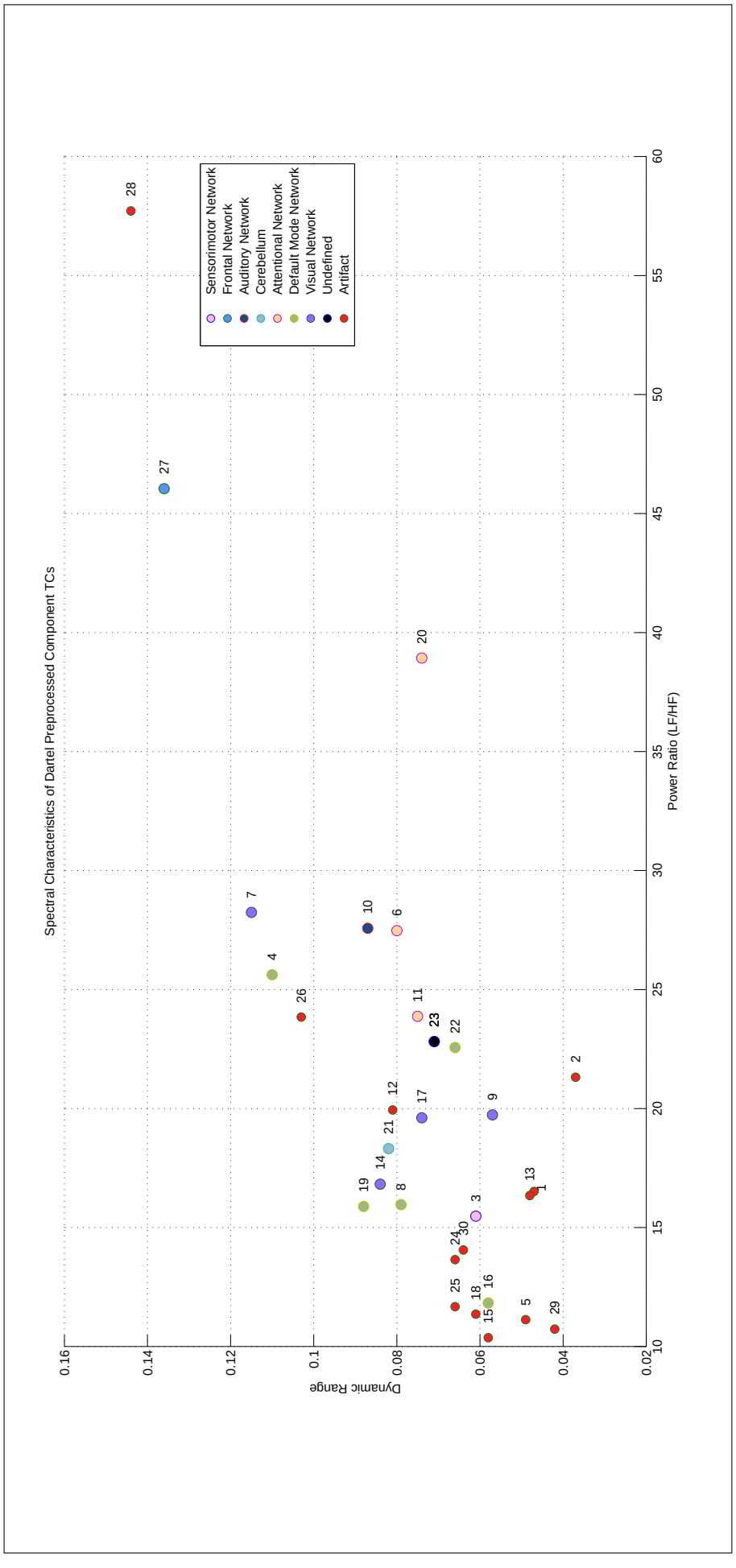

Figure 3.33 Dynamic range and power ratio graphs of components

4. DISCUSSION AND CONCLUSION

The fMRI data in the study is gathered from 64 elderly subjects, having AD, MCI or being healthy, while attending an optimized auditory oddball task. After the initial check of the structural and functional images, 16 subjects are found to be qualified enough for the analysis. Although statistically better results can be obtained with 12 people for each group at least, the study is continued with total of 16 subjects in order to examine the highest quality of data as a pilot study.

The data is first skull-stripped and then preprocessed in two different ways with DARTEL method and regular method, explained in detail in methods chapter (Subsection 2.2.3). The reason for using two different ways is to see the effects of preprocessing on proceeding steps. It is known that ICA is affected by the preprocessing steps [29]. When subtle spatial differences are researched, image registration and normalization becomes an important element in the study, especially if there is a mismatch between the template population and the subject group. For this purpose, DARTEL is found to be superior in accurateness when compared to regular coregistration and normalization processes [23, 25]. Moreover, it can be applied via SPM written mostly by Karl Friston and John Ashburner.

The chosen group ICA necessitates further preprocessing due to the statistical postulates of the algorithms and the computational load. Thus, the following step includes intensity normalization, subject-level PCA, whitening, temporal concatenation and group-level PCA. After the preprocessing, the data are decomposed into independent components via Infomax algorithm. This algorithm is actually applied for 30 times with ICASSO in order to get the most stable results. The components are then backreconstructed into subject-wise data. Consequently, the total outcome becomes the aggregate components (having spatial maps and temporal courses) belonging to all of the subjects and components belonging to each of the subjects.

The above mentioned steps are applied to 2 differently grouped subject data with the component numbers of 20, 25, 30, 40, 50, 60 and 70. Firstly, the subjects are grouped as AD, MCI and CT before the ICA in order to get separate results for each group. Secondly, all of the subjects are grouped as AD, MCI and CT after the ICA of all subjects as one group. Neurologists compared the outcomes and favored the latter grouping with 30 components. The number of components that can be extracted from the data are also estimated by an algorithm utilizing MDL criteria. This is done in order to check the liability of the current algorithmic method, offered as a solution for the component number selection problem. The component number difference between the average numbers is 5 since the MDL defined 25 as the average number of components that can be extracted from the data. The difference in selection can be explained by the sub-network effect of higher component numbers and the possibility of underestimation of the algorithm. When the networks of 25 component ICA and 30 component ICA are compared, some important networks, such as DMNs, are found to be mixed with the artifacts. On the other hand, when the networks having higher components, particularly 70 components, are explored, networks which are mostly separated from the artifact components such as the basal ganglia network from the vetricular activation artifact are found. However, the 30 component approach is adopted since the separation of components from each other is not limited with the artifact containing ones.

There are two different 30 component ICA results due to different preprocessing steps as mentioned above. These two different 30 component sets have also an ICASSO history, which means that there are $2 \times 30 \times 30$ result set, as the ICA process is applied 30 times with ICASSO. Each 30×30 component set is clustered and the centrotypes are chosen in order to get the most stable outcomes since ICA is a stochastic process.

After considering the overall effect of preprocessing steps, the main network sections in results chapter are designed with the components of the data preprocessed with DARTEL. In summary, 9 different network groups are found based on the previous studies [43, 67, 12, 72]; namely:

1. **Attentional Network:** 6th, 11th and 20th components
2. **Auditory Network:** 10th component
3. **Cerebellum:** 21st component
4. **Default Mode Network:** 4th, 8th, 16th, 19th and 22nd components
5. **Frontal Network:** 27th component
6. **Sensorimotor Network:** 3rd component
7. **Visual Network:** 7th, 9th, 14th and 17th components
8. **Unclassified Network:** 23th component
9. **Artifact related components:** 1st, 2nd, 5th, 12th, 13th, 15th, 18th, 24th, 25th, 26th, 28th, 29th and 30th components

For attentional network group, the expectation was to find dorsal attention network and salience network among others. However, these two common networks are missing in this study. On the other hand, there is one unclassified network due to its resemblance to 4 different networks mentioned in the literature (Section 3.9). This may be due to the quality of the clinical data and the elderly population.

Clues about the extension of artifact contamination in a component can be gained via the spectral analysis of the temporal courses of the components [43]. For that, three measures, such as dynamic range and power ratios in addition to the usual spectral graph including all of the subjects data can be used. In this study, this analysis is applied to component time courses in two different ways. The difference between the two ways is an additional detrending step, applied before the spectral analysis. The results are positive only for the trendy temporal courses of the components. This result is expected as the experiment has a task. The graph depicting the dynamic ranges and power ratios as well as the spectrums of the components are checked while determining the artifact related components. The main criteria for selection is the literature about the components of the movement, respiration, cardiac pulse or known vascular and

cerebrospinal fluid or air filled areas. However, the analytic metrics help when there is a dilemma about the artifact percentage of a component.

When the connectivity between networks are considered, the strengths do not go higher than 0.4 for the z-scores. However, they are worth to be reported as in the literature [43]. Additionally, this may indicate age and pathology related factors if the quality of the data issue is eliminated. The connectivities, whose coefficients are higher than 0.3, can be summarized as follows (Figure 4.1):

1. Positive correlation between visual and frontal networks: The related networks have middle prefrontal gyrus and visual association cortex as parts of them, as can be seen from the results chapter. Middle prefrontal cortex is found to function as a top-down control mechanism for the visual assocciation cortex especially when a visual working memory task is attended. Thus, they are said to be functionally correlated [90]. Although the task in this study is irrelevant, it is possible that this connection may be related with this mechanism.

2. Both positive and negative correlation between DMN and visual networks: They are found to be coupled when there is a need for suppression of task irrelevant information during a visual working memory task. Therefore, it may even be the coupled effort to suppress distraction of visual stimulation together with internally generated information [78].

3. Both positive and negative correlation between DMN and attentional networks: The attentional network in this case is mostly consisted of precuneus. As mentioned in the results chapter, this component may have positive correlations with the DMN during rest, and even become a part of DMN [71]. It can also have negative correlations with the DMN indirectly since it is found to be mostly correlated with fronto-parietal network during task. Although, there are no significant correlations above 0.3 between DMN and fronto-parietal network in this study, this outcome is important.

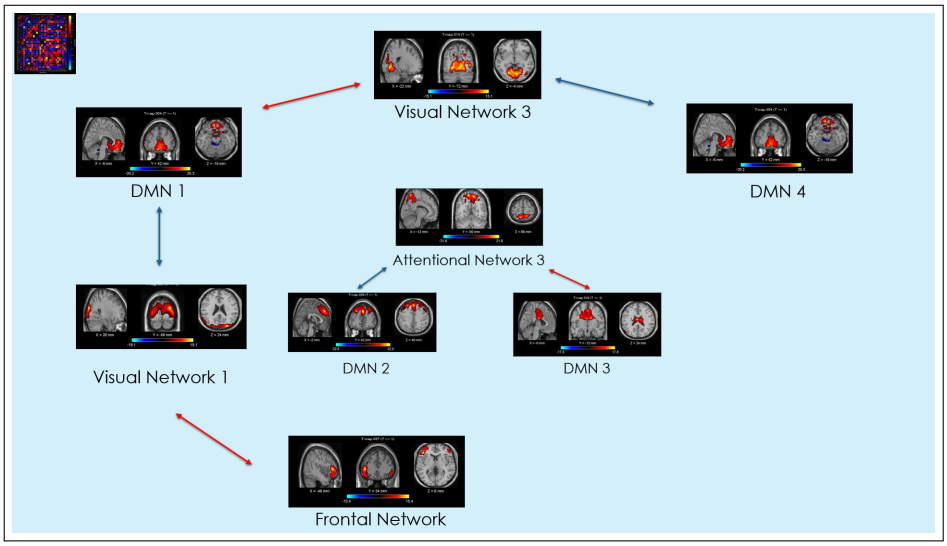

Figure 4.1 Functional connectivity summary

When the spatial maps, functional connectivities and spectral bins of AD, MCI and CT are compared in a multivariate fashion via MANCOVA, 6th (Attentional Network 1), 16th (DMN 3) and 20th (Attentional Network 3) components for spatial maps; 9th (Visual Network 2) for the spectral differences are found to have differences whereas there is no result for the functional connectivity comparison. The results being not as strong as expected might be due to the quality of the data.

In order to have more detailed explanation over multivarite tests, univariate tests are done. For the spatial maps, FDR is used for multiple comparison correction. The results include regions in the 16th component (DMN 3), between controls and AD patients in white matter of sub-gyral frontal lobe, and 20th component (Attentional Network 3), between MCI and AD patients in precuneus. Unfortunately, no conclusions can be made upon the spatial map differences of AD and MCI since the significant voxels do not exceed 5-voxel threshold.

As a novelty in the field of AD and MCI, temporal sorting is done in order to find the modulation of the task upon the components via multiple regression with the target stimuli and normal stimuli regressors as well as their time derivatives. Additionally, the beta values of the regression coefficients are compared in 8 different ways in order to detect group or regressor differences. In summary, the regressor type affects the order

of the components and the beta value comparison outcomes. As for the group-wise comparisons, it can be said that all of the network sets have some difference between various couplings of AD, MCI, and CT when various couplings of regressors are taken into account. The bigger picture can be seen from the Figure 4.2.

To conclude, the aim of this study was to find a bio-marker for differentiating AD and MCI from the healthy subjects via ICA as well as studying the effect of image registration for this analysis as a side aspect. For that, a preprocessing step utilizing a diffeomorphic registration algorithm (DARTEL) is used before the group ICA analysis. To perform the group inference, the group ICA analysis concatenates the subjects temporally into a single group. Later, by backreconstruction, the subject information is obtained. As for the further analysis, the data is inspected both spatially and temporally. The expected results were mostly for the spatial maps of the components at the beginning; however, temporal course analysis gave the most abundant outcomes. The overall results are insufficient in differentiating between the diseases via spatial maps. On the contrary, since the component temporal course regression of AD and MCI for the oddball paradigm is novel in the field, it may suggest a new frame for the disease pathology differentiation. As for the future interest, this finding should be supported by a longitudinal study having both task related and resting state data. Moreover, the quality and quantity of longitudinal data should be considered beforehand. The first step after the data collection of about 100 subjects would be to utilize a clustering analysis method. By doing so, the variances of β values can be checked whether they exist for a larger sample. Moreover, the success of the metrics to be calculated from those variances can be assessed for their validity in differentiating the diseases.

Attentional Network 1

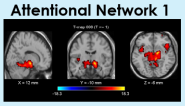

Targets
AD>MCI; p=0.02 CT>MCI; p=0.008

***Attentional Network 3**

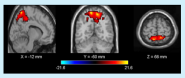

Targets	Normals	Normals + $dt_{Nor.}$	For all regressors
MCI>AD; p=0.05	MCI>AD; p=0.003	CT>AD; p=0.03 MCI>AD; p=0.0007	MCI>AD; p=0.02

Auditory Network

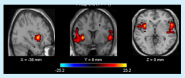

AD>CT & Targets>Normals	MCI>CT & Targets>Normals
P=0.02	p=0.0046

Sensorimotor Network

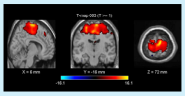

AD>CT & Targets>Normals	MCI>CT & Targets>Normals p=0.0046
p=0.058	p=0.009

* Means that Attentional Network 3 also has two-way ANOVA results with the contrasts MCI>CT & Targets>Normals, and p=0.002

Cerebellum

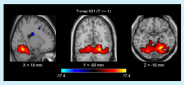

Targets	Targets + $dt_{Tar.}$	Normals and Targets	For all regressors
CT>AD; p=0.002 CT>MCI; p=0.008	CT>AD; p=0.03 MCI>AD; p=0.003	CT>AD; p=0.01 CT>MCI; p=0.03	MCI>AD; p=0.04

DMN 1

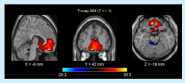

Targets + $dt_{Tar.}$	Normals	AD>CT & AD>MCI & MCI>CT & Targets>Normal
MCI>AD; p=0.058	CT>AD; p=0.04 CT>MCI; p=0.02	p=0.005, with negative t value p=0.0047, with negative t value p=0.05, with negative t value

DMN 2

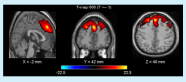

Normals	Normals + $dt_{Nor.}$
AD>CT; p=0.05 AD>MCI; p=0.009	AD>MCI; p=0.02

DMN 4

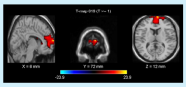

Normals	Normals + $dt_{Nor.}$	For all regressors
CT>AD; p=0.03 MCI>AD; p=0.03	CT>AD; p=0.03 MCI>AD; p=0.03	MCI>AD; p=0.05

Visual Network 3

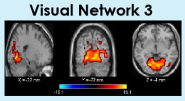

Targets	Normals and Target
AD>CT; p=0.03 AD>MCI; p=0.004	AD>MCI; p=0.03

Visual Network 4

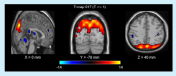

For all regressors	AD>CT & Targets>Normals
CT>AD; p=0.03	p=0.01

Unclassified

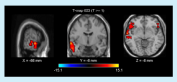

Targets + $dt_{Tar.}$	AD>CT & Targets>Normals
CT>AD; p=0.04	p=0.02, with negative t value

Figure 4.2 The summary of the β value statistics

5. APPENDIX

5.1 Relation of Test Outcomes with the Experiment Conditions

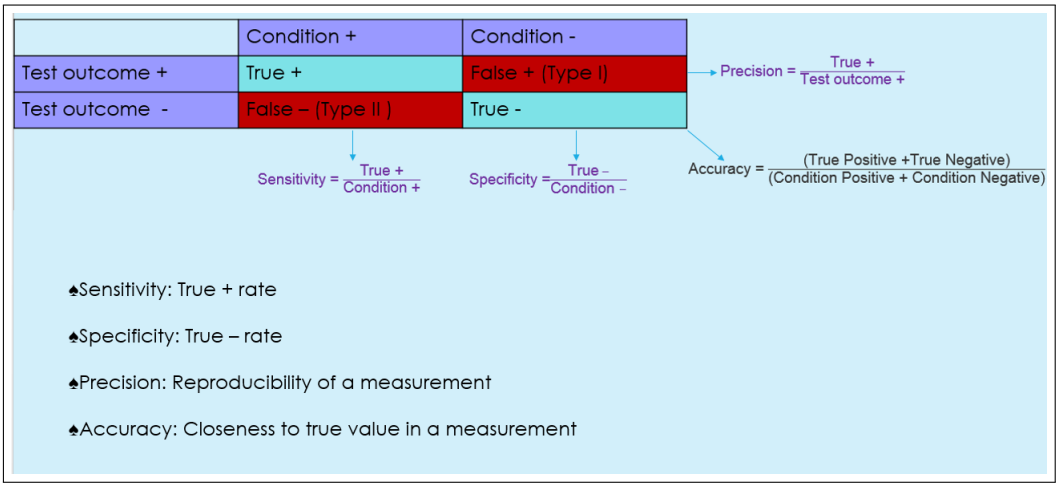

Figure 5.1 Relation of Test Outcomes with the Experiment Conditions

5.2 Software Packages for Preprocessing and Processing the (f)MRI Data

1. AFNI (http://afni.nimh.nih.gov/afni/),
2. FSL (http://fsl.fmrib.ox.ac.uk/fsl/fslwiki/),
3. Brain Voyager (http://www.brainvoyager.com/),
4. Brain Suite (http://brainsuite.org/),
5. SPM (http://www.fil.ion.ucl.ac.uk/spm/).

5.3 Anatomical Brain Regions

In Figure 5.3, the anatomical regions of brain are depicted.

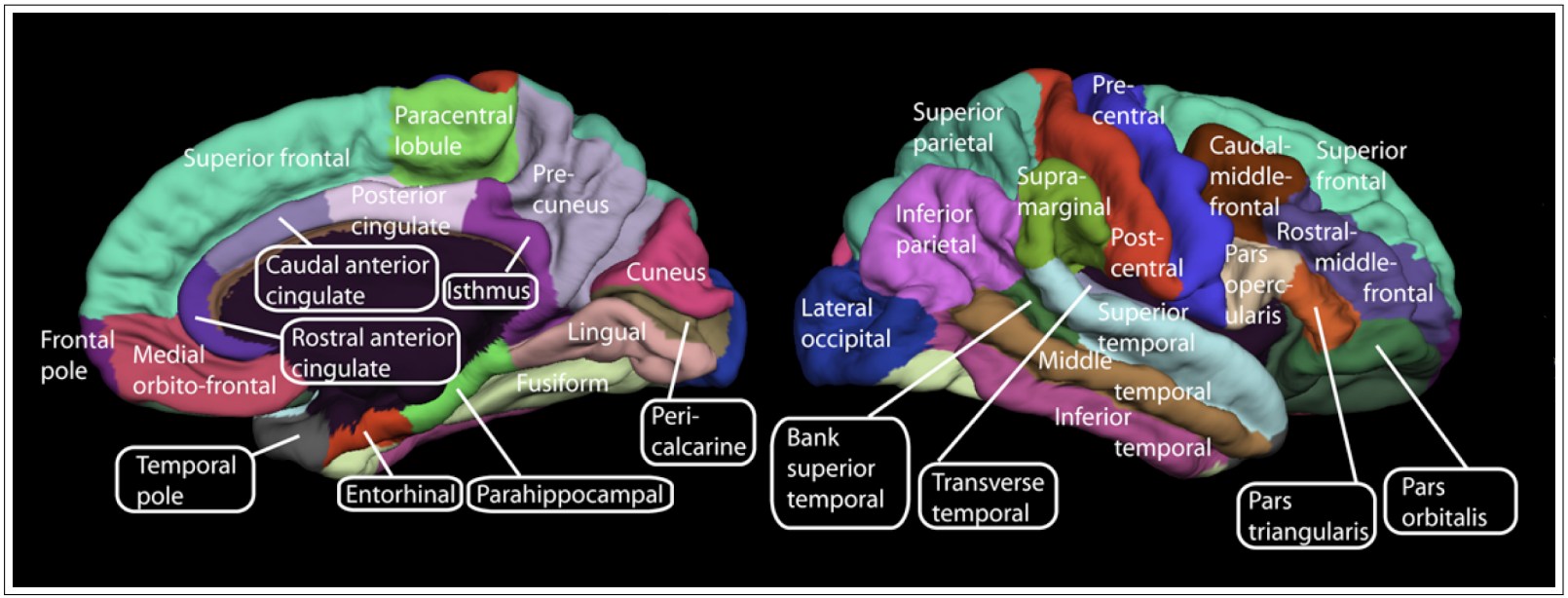

Figure 5.2 Anatomical brain regions [5]

REFERENCES

1. Kandel, E. R., J. H. Schwartz, T. M. Jessell, S. A. Siegelbaum, and A. J. Hudspeth, eds., *Principles of Neural Science*, McGraw-Hill Medical, 5th editio ed., 2013.

2. Mulert, C., and L. Lemieux, eds., *EEG - fMRI*, Berlin, Heidelberg: Springer Berlin Heidelberg, 2010.

3. Lindquist, M. A., "The Statistical Analysis of fMRI Data," *Statistical Science*, Vol. 23, pp. 439–464, Nov. 2008.

4. Hyvärinen, a., and E. Oja, "Independent component analysis: algorithms and applications.," *Neural networks : the official journal of the International Neural Network Society*, Vol. 13, no. 4-5, pp. 411–30, 2000.

5. Hagmann, P., L. Cammoun, X. Gigandet, R. Meuli, C. J. Honey, V. J. Wedeen, and O. Sporns, "Mapping the structural core of human cerebral cortex.," *PLoS biology*, Vol. 6, p. e159, July 2008.

6. Liu, Z., Y. Zhang, H. Yan, L. Bai, R. Dai, W. Wei, C. Zhong, T. Xue, H. Wang, Y. Feng, Y. You, X. Zhang, and J. Tian, "Altered topological patterns of brain networks in mild cognitive impairment and Alzheimer's disease: a resting-state fMRI study.," *Psychiatry research*, Vol. 202, pp. 118–25, May 2012.

7. Liu, Y., K. Wang, C. Yu, Y. He, Y. Zhou, M. Liang, L. Wang, and T. Jiang, "Regional homogeneity, functional connectivity and imaging markers of Alzheimer's disease: a review of resting-state fMRI studies.," *Neuropsychologia*, Vol. 46, pp. 1648–56, Jan. 2008.

8. Ballard, C., S. Gauthier, A. Corbett, C. Brayne, D. Aarsland, and E. Jones, "Alzheimer's disease.," *Lancet*, Vol. 377, pp. 1019–31, Mar. 2011.

9. Gauthier, S., B. Reisberg, M. Zaudig, R. C. Petersen, K. Ritchie, K. Broich, S. Belleville, H. Brodaty, D. Bennett, H. Chertkow, J. L. Cummings, M. de Leon, H. Feldman, M. Ganguli, H. Hampel, P. Scheltens, M. C. Tierney, P. Whitehouse, and B. Winblad, "Mild cognitive impairment.," *Lancet*, Vol. 367, pp. 1262–70, Apr. 2006.

10. Brier, M. R., J. B. Thomas, and B. M. Ances, "Network dysfunction in Alzheimer's disease: refining the disconnection hypothesis.," *Brain connectivity*, Vol. 4, pp. 299–311, June 2014.

11. Klupp, E., S. Förster, T. Grimmer, M. Tahmasian, I. Yakushev, C. Sorg, B. H. Yousefi, and A. Drzezga, "In Alzheimer's disease, hypometabolism in low-amyloid brain regions may be a functional consequence of pathologies in connected brain regions.," *Brain connectivity*, Vol. 4, pp. 371–83, June 2014.

12. Seeley, W. W., V. Menon, A. F. Schatzberg, J. Keller, G. H. Glover, H. Kenna, A. L. Reiss, and M. D. Greicius, "Dissociable intrinsic connectivity networks for salience processing and executive control.," *The Journal of neuroscience : the official journal of the Society for Neuroscience*, Vol. 27, pp. 2349–56, Feb. 2007.

13. Logothetis, N. K., "What we can do and what we cannot do with fMRI.," *Nature*, Vol. 453, pp. 869–78, June 2008.

14. Gasiorowicz, S., *Quantum Physics, Third Edition [Hardcover]*, Wiley, third edit ed., 2003.

15. Filippi, M., ed., *fMRI Techniques and Protocols*, Vol. 41 of *Neuromethods*, Totowa, NJ: Humana Press, 2009.

16. Prince, J. L., and J. Links, *Medical Imaging Signals and Systems*, Prentice Hall, 1st ed., 2005.

17. Haller, S., and A. J. Bartsch, "Pitfalls in FMRI.," *European radiology*, Vol. 19, pp. 2689–706, Nov. 2009.

18. Lindquist, M. A., and T. D. Wager, "Validity and power in hemodynamic response modeling: a comparison study and a new approach.," *Human brain mapping*, Vol. 28, pp. 764–84, Aug. 2007.

19. Lindquist, M. A., J. Meng Loh, L. Y. Atlas, and T. D. Wager, "Modeling the hemodynamic response function in fMRI: efficiency, bias and mis-modeling.," *NeuroImage*, Vol. 45, pp. S187–98, Mar. 2009.

20. Biswal, B. B., "Resting state fMRI: a personal history.," *NeuroImage*, Vol. 62, pp. 938–44, Aug. 2012.

21. Lindquist, M. a., B. Caffo, and C. Crainiceanu, "Ironing out the statistical wrinkles in "ten ironic rules".," *NeuroImage*, Vol. 81, pp. 499–502, Nov. 2013.

22. Satterthwaite, T. D., M. a. Elliott, R. T. Gerraty, K. Ruparel, J. Loughead, M. E. Calkins, S. B. Eickhoff, H. Hakonarson, R. C. Gur, R. E. Gur, and D. H. Wolf, "An improved framework for confound regression and filtering for control of motion artifact in the preprocessing of resting-state functional connectivity data.," *NeuroImage*, Vol. 64, pp. 240–56, Jan. 2013.

23. Ashburner, J., "A fast diffeomorphic image registration algorithm.," *NeuroImage*, Vol. 38, pp. 95–113, Oct. 2007.

24. Ashburner, J., and K. J. Friston, "Diffeomorphic registration using geodesic shooting and Gauss-Newton optimisation.," *NeuroImage*, Vol. 55, pp. 954–67, Apr. 2011.

25. Klein, A., J. Andersson, B. A. Ardekani, J. Ashburner, B. Avants, M.-C. Chiang, G. E. Christensen, D. L. Collins, J. Gee, P. Hellier, J. H. Song, M. Jenkinson, C. Lepage, D. Rueckert, P. Thompson, T. Vercauteren, R. P. Woods, J. J. Mann, and R. V. Parsey, "Evaluation of 14 nonlinear deformation algorithms applied to human brain MRI registration.," *NeuroImage*, Vol. 46, pp. 786–802, July 2009.

26. Takahashi, R., K. Ishii, N. Miyamoto, T. Yoshikawa, K. Shimada, S. Ohkawa, T. Kakigi, and K. Yokoyama, "Measurement of gray and white matter atrophy in dementia with Lewy bodies using diffeomorphic anatomic registration through exponentiated lie algebra: A comparison with conventional voxel-based morphometry.," *AJNR. American journal of neuroradiology*, Vol. 31, pp. 1873–8, Nov. 2010.

27. Fischmeister, F. P. S., I. Höllinger, N. Klinger, a. Geissler, M. C. Wurnig, E. Matt, J. Rath, S. D. Robinson, S. Trattnig, and R. Beisteiner, "The benefits of skull stripping in the normalization of clinical fMRI data.," *NeuroImage. Clinical*, Vol. 3, pp. 369–80, Jan. 2013.

28. Strother, S., "Evaluating fMRI preprocessing pipelines," *IEEE Engineering in Medicine and Biology Magazine*, Vol. 25, pp. 27–41, Mar. 2006.

29. Andronache, A., C. Rosazza, D. Sattin, M. Leonardi, L. D'Incerti, and L. Minati, "Impact of functional MRI data preprocessing pipeline on default-mode network detectability in patients with disorders of consciousness.," *Frontiers in neuroinformatics*, Vol. 7, p. 16, Jan. 2013.

30. Siegel, J. S., J. D. Power, J. W. Dubis, A. C. Vogel, J. a. Church, B. L. Schlaggar, and S. E. Petersen, "Statistical improvements in functional magnetic resonance imaging analyses produced by censoring high-motion data points.," *Human brain mapping*, Vol. 35, pp. 1981–96, May 2014.

31. Cheng, H., and A. Puce, "Reducing respiratory effect in motion correction for EPI images with sequential slice acquisition order.," *Journal of neuroscience methods*, Vol. 227, pp. 83–9, Apr. 2014.

32. Bianchi, M. T., V. S. Caviness, and S. S. Cash, eds., *Network Approaches to Diseases of the Brain*, UAE: Bentham Science Publishers, 2012.

33. van den Heuvel, M. P., and H. E. Hulshoff Pol, "Exploring the brain network: a review on resting-state fMRI functional connectivity.," *European neuropsychopharmacology : the journal of the European College of Neuropsychopharmacology*, Vol. 20, pp. 519–34, Aug. 2010.

34. Damoiseaux, J. S., and M. D. Greicius, "Greater than the sum of its parts: a review of studies combining structural connectivity and resting-state functional connectivity.," *Brain structure & function*, Vol. 213, pp. 525–33, Oct. 2009.

35. Rubinov, M., and O. Sporns, "Complex network measures of brain connectivity: uses and interpretations.," *NeuroImage*, Vol. 52, pp. 1059–69, Sept. 2010.

36. Li, K., L. Guo, J. Nie, G. Li, and T. Liu, "Review of methods for functional brain connectivity detection using fMRI.," *Computerized medical imaging and graphics : the official journal of the Computerized Medical Imaging Society*, Vol. 33, pp. 131–9, Mar. 2009.

37. Rodgers, J. L., W. A. Nicewander, and L. Toothaker, "Linearly independent, orthogonal, and uncorrelated variables," *The American Statistician*, Vol. 38, no. 2, pp. 133–134, 1984.

38. Hyvärinen, A., J. Karhunen, and E. Oja, *Independent Component Analysis*, John Wiley & Sons, 2004.

39. Erhardt, E. B., E. A. Allen, E. Damaraju, and V. D. Calhoun, "On network derivation, classification, and visualization: a response to Habeck and Moeller.," *Brain connectivity*, Vol. 1, pp. 105–10, Jan. 2011.

40. Calhoun, V. D., K. A. Kiehl, and G. D. Pearlson, "Modulation of temporally coherent brain networks estimated using ICA at rest and during cognitive tasks.," *Human brain mapping*, Vol. 29, pp. 828–38, July 2008.

41. Venkataraman, A., K. R. A. Van Dijk, R. L. Buckner, and P. Golland, "Exploring functional connectivity in fMRI via clustering," Apr. 2009.

42. Liu, D., N. Zhong, and Y. Qin, "Exploring functional connectivity networks in fmri data using clustering analysis," in *Brain Informatics* (Hu, B., J. Liu, L. Chen, and N. Zhong, eds.), Vol. 6889 of *Lecture Notes in Computer Science*, pp. 148–159, Springer Berlin Heidelberg, 2011.

43. Allen, E. A., E. B. Erhardt, E. Damaraju, W. Gruner, J. M. Segall, R. F. Silva, M. Havlicek, S. Rachakonda, J. Fries, R. Kalyanam, A. M. Michael, A. Caprihan, J. A. Turner, T. Eichele, S. Adelsheim, A. D. Bryan, J. Bustillo, V. P. Clark, S. W. Feldstein Ewing, F. Filbey, C. C. Ford, K. Hutchison, R. E. Jung, K. A. Kiehl, P. Kodituwakku, Y. M. Komesu, A. R. Mayer, G. D. Pearlson, J. P. Phillips, J. R. Sadek, M. Stevens, U. Teuscher, R. J. Thoma, and V. D. Calhoun, "A baseline for the multivariate comparison of resting-state networks.," *Frontiers in systems neuroscience*, Vol. 5, p. 2, Jan. 2011.

44. Bell, A. J., and T. J. Sejnowski, "An Information-Maximization Approach to Blind Separation and Blind Deconvolution," *Neural Computation*, Vol. 7, pp. 1129–1159, Nov. 1995.

45. Hyvärinen, A., and E. Oja, "A Fast Fixed-Point Algorithm for Independent Component Analysis," *Neural Computation*, Vol. 9, pp. 1483–1492, Oct. 1997.

46. Beckmann, C. F., and S. M. Smith, "Probabilistic independent component analysis for functional magnetic resonance imaging.," *IEEE transactions on medical imaging*, Vol. 23, pp. 137–52, Feb. 2004.

47. Beckmann, C. F., M. DeLuca, J. T. Devlin, and S. M. Smith, "Investigations into resting-state connectivity using independent component analysis.," *Philosophical transactions of the Royal Society of London. Series B, Biological sciences*, Vol. 360, pp. 1001–13, May 2005.

48. Calhoun, V. D., J. Liu, and T. Adali, "A review of group ICA for fMRI data and ICA for joint inference of imaging, genetic, and ERP data.," *NeuroImage*, Vol. 45, pp. S163–72, Mar. 2009.

49. Correa, N., T. Adali, and V. D. Calhoun, "Performance of blind source separation algorithms for fMRI analysis using a group ICA method.," *Magnetic resonance imaging*, Vol. 25, pp. 684–94, June 2007.

50. Schöpf, V., C. Windischberger, C. H. Kasess, R. Lanzenberger, and E. Moser, "Group ICA of resting-state data: a comparison.," *Magma (New York, N.Y.)*, Vol. 23, pp. 317–25, Dec. 2010.

51. Erhardt, E. B., S. Rachakonda, E. J. Bedrick, E. A. Allen, T. Adali, and V. D. Calhoun, "Comparison of multi-subject ICA methods for analysis of fMRI data.," *Human brain mapping*, Vol. 32, pp. 2075–95, Dec. 2011.

52. Lindquist, M. A., "Multiple Comparisons in Neuroimaging," 2011.

53. Rissanen, J., "Modeling by shortest data description," *Automatica*, Vol. 14, pp. 465–471, Sept. 1978.

54. Hui, M., J. Li, X. Wen, L. Yao, and Z. Long, "An empirical comparison of information-theoretic criteria in estimating the number of independent components of fMRI data.," *PloS one*, Vol. 6, p. e29274, Jan. 2011.

55. Power, J. D., A. L. Cohen, S. M. Nelson, G. S. Wig, K. A. Barnes, J. A. Church, A. C. Vogel, T. O. Laumann, F. M. Miezin, B. L. Schlaggar, and S. E. Petersen, "Functional network organization of the human brain.," *Neuron*, Vol. 72, pp. 665–78, Nov. 2011.

56. Yeo, B. T. T., F. M. Krienen, J. Sepulcre, M. R. Sabuncu, D. Lashkari, M. Hollinshead, J. L. Roffman, J. W. Smoller, L. Zöllei, J. R. Polimeni, B. Fischl, H. Liu, and R. L. Buckner, "The organization of the human cerebral cortex estimated by intrinsic functional connectivity.," *Journal of neurophysiology*, Vol. 106, pp. 1125–65, Sept. 2011.

57. Di, X., and B. B. Biswal, "Modulatory interactions between the default mode network and task positive networks in resting-state.," *PeerJ*, Vol. 2, p. e367, Jan. 2014.

58. Lückmann, H. C., H. I. L. Jacobs, and A. T. Sack, "The cross-functional role of frontoparietal regions in cognition: internal attention as the overarching mechanism.," *Progress in neurobiology*, Vol. 116, pp. 66–86, May 2014.

59. Fox, M. D., A. Z. Snyder, J. L. Vincent, M. Corbetta, D. C. Van Essen, and M. E. Raichle, "The human brain is intrinsically organized into dynamic, anticorrelated functional networks.," *Proceedings of the National Academy of Sciences of the United States of America*, Vol. 102, pp. 9673–8, July 2005.

60. Laird, A. R., P. M. Fox, S. B. Eickhoff, J. A. Turner, K. L. Ray, D. R. McKay, D. C. Glahn, C. F. Beckmann, S. M. Smith, and P. T. Fox, "Behavioral interpretations of intrinsic connectivity networks.," *Journal of cognitive neuroscience*, Vol. 23, pp. 4022–37, Dec. 2011.

61. Society for Neuroscience, *Brain Facts book - BrainFacts.org*, The Kavli Foundation, Gatsby, Society for Neuroscience, 2012.

62. Donnelly, L., "The brain: functional divisions," *Anaesthesia & Intensive Care Medicine*, Vol. 15, pp. 195–200, Apr. 2014.

63. Nieuwenhuys, R., "The insular cortex: a review.," *Progress in brain research*, Vol. 195, pp. 123–63, Jan. 2012.

64. Nachev, P., C. Kennard, and M. Husain, "Functional role of the supplementary and pre-supplementary motor areas.," *Nature reviews. Neuroscience*, Vol. 9, pp. 856–69, Nov. 2008.

65. Spreng, R. N., J. Sepulcre, G. R. Turner, W. D. Stevens, and D. L. Schacter, "Intrinsic architecture underlying the relations among the default, dorsal attention, and frontoparietal control networks of the human brain.," *Journal of cognitive neuroscience*, Vol. 25, pp. 74–86, Jan. 2013.

66. Sridharan, D., D. J. Levitin, and V. Menon, "A critical role for the right fronto-insular cortex in switching between central-executive and default-mode networks.," *Proceedings of the National Academy of Sciences of the United States of America*, Vol. 105, pp. 12569–74, Aug. 2008.

67. Smith, S. M., P. T. Fox, K. L. Miller, D. C. Glahn, P. M. Fox, C. E. Mackay, N. Filippini, K. E. Watkins, R. Toro, A. R. Laird, and C. F. Beckmann, "Correspondence of the brain's functional architecture during activation and rest.," *Proceedings of the National Academy of Sciences of the United States of America*, Vol. 106, pp. 13040–5, Aug. 2009.

68. Cole, M. W., J. R. Reynolds, J. D. Power, G. Repovs, A. Anticevic, and T. S. Braver, "Multi-task connectivity reveals flexible hubs for adaptive task control.," *Nature neuroscience*, Vol. 16, pp. 1348–55, Sept. 2013.

69. Margulies, D. S., J. L. Vincent, C. Kelly, G. Lohmann, L. Q. Uddin, B. B. Biswal, A. Villringer, F. X. Castellanos, M. P. Milham, and M. Petrides, "Precuneus shares intrinsic functional architecture in humans and monkeys.," *Proceedings of the National Academy of Sciences of the United States of America*, Vol. 106, pp. 20069–74, Nov. 2009.

70. Zhang, S., and C.-s. R. Li, "Functional connectivity mapping of the human precuneus by resting state fMRI.," *NeuroImage*, Vol. 59, pp. 3548–62, Feb. 2012.

71. Utevsky, A. V., D. V. Smith, and S. A. Huettel, "Precuneus is a functional core of the default-mode network.," *The Journal of neuroscience : the official journal of the Society for Neuroscience*, Vol. 34, pp. 932–40, Jan. 2014.

72. Damoiseaux, J. S., S. A. R. B. Rombouts, F. Barkhof, P. Scheltens, C. J. Stam, S. M. Smith, and C. F. Beckmann, "Consistent resting-state networks across healthy subjects.," *Proceedings of the National Academy of Sciences of the United States of America*, Vol. 103, pp. 13848–53, Sept. 2006.

73. Veer, I. M., C. F. Beckmann, M.-J. van Tol, L. Ferrarini, J. Milles, D. J. Veltman, A. Aleman, M. A. van Buchem, N. J. van der Wee, and S. A. R. B. Rombouts, "Whole brain resting-state analysis reveals decreased functional connectivity in major depression.," *Frontiers in systems neuroscience*, Vol. 4, Jan. 2010.

74. Heine, L., A. Soddu, F. Gómez, A. Vanhaudenhuyse, L. Tshibanda, M. Thonnard, V. Charland-Verville, M. Kirsch, S. Laureys, and A. Demertzi, "Resting state networks and consciousness: alterations of multiple resting state network connectivity in physiological, pharmacological, and pathological consciousness States.," *Frontiers in psychology*, Vol. 3, p. 295, Jan. 2012.

75. Buckner, R. L., J. R. Andrews-Hanna, and D. L. Schacter, "The brain's default network: anatomy, function, and relevance to disease.," *Annals of the New York Academy of Sciences*, Vol. 1124, pp. 1–38, Mar. 2008.

76. Hasenkamp, W., C. D. Wilson-Mendenhall, E. Duncan, and L. W. Barsalou, "Mind wandering and attention during focused meditation: a fine-grained temporal analysis of fluctuating cognitive states.," *NeuroImage*, Vol. 59, pp. 750–60, Jan. 2012.

77. Li, W., W. Qin, H. Liu, L. Fan, J. Wang, T. Jiang, and C. Yu, "Subregions of the human superior frontal gyrus and their connections.," *NeuroImage*, Vol. 78, pp. 46–58, Sept. 2013.

78. Chadick, J. Z., and A. Gazzaley, "Differential coupling of visual cortex with default or frontal-parietal network based on goals.," *Nature neuroscience*, Vol. 14, pp. 830–2, July 2011.

79. Saur, D., B. W. Kreher, S. Schnell, D. Kümmerer, P. Kellmeyer, M.-S. Vry, R. Umarova, M. Musso, V. Glauche, S. Abel, W. Huber, M. Rijntjes, J. Hennig, and C. Weiller, "Ventral and dorsal pathways for language.," *Proceedings of the National Academy of Sciences of the United States of America*, Vol. 105, pp. 18035–40, Nov. 2008.

80. Pascual, B., J. C. Masdeu, M. Hollenbeck, N. Makris, R. Insausti, S.-L. Ding, and B. C. Dickerson, "Large-Scale Brain Networks of the Human Left Temporal Pole: A Functional Connectivity MRI Study.," *Cerebral cortex (New York, N.Y. : 1991)*, pp. bht260–, Sept. 2013.

81. Visser, M., E. Jefferies, K. V. Embleton, and M. A. Lambon Ralph, "Both the middle temporal gyrus and the ventral anterior temporal area are crucial for multimodal semantic processing: distortion-corrected fMRI evidence for a double gradient of information convergence in the temporal lobes.," *Journal of cognitive neuroscience*, Vol. 24, pp. 1766–78, Aug. 2012.

82. Rosazza, C., and L. Minati, "Resting-state brain networks: literature review and clinical applications.," *Neurological sciences : official journal of the Italian Neurological Society and of the Italian Society of Clinical Neurophysiology*, Vol. 32, pp. 773–85, Oct. 2011.

83. Acheson, D. J., and P. Hagoort, "Stimulating the brain's language network: syntactic ambiguity resolution after TMS to the inferior frontal gyrus and middle temporal gyrus.," *Journal of cognitive neuroscience*, Vol. 25, pp. 1664–77, Oct. 2013.

84. Bigler, E. D., S. Mortensen, E. S. Neeley, S. Ozonoff, L. Krasny, M. Johnson, J. Lu, S. L. Provencal, W. McMahon, and J. E. Lainhart, "Superior temporal gyrus, language function, and autism.," *Developmental neuropsychology*, Vol. 31, pp. 217–38, Jan. 2007.

85. Lee, J. E., E. D. Bigler, A. L. Alexander, M. Lazar, M. B. DuBray, M. K. Chung, M. Johnson, J. Morgan, J. N. Miller, W. M. McMahon, J. Lu, E.-K. Jeong, and J. E. Lainhart, "Diffusion tensor imaging of white matter in the superior temporal gyrus and temporal stem in autism.," *Neuroscience letters*, Vol. 424, pp. 127–32, Sept. 2007.

86. Deschamps, I., S. R. Baum, and V. L. Gracco, "On the role of the supramarginal gyrus in phonological processing and verbal working memory: evidence from rTMS studies.," *Neuropsychologia*, Vol. 53, pp. 39–46, Jan. 2014.

87. Macuga, K. L., and S. H. Frey, "Selective responses in right inferior frontal and supramarginal gyri differentiate between observed movements of oneself vs. another.," *Neuropsychologia*, Vol. 49, pp. 1202–7, Apr. 2011.

88. Silani, G., C. Lamm, C. C. Ruff, and T. Singer, "Right supramarginal gyrus is crucial to overcome emotional egocentricity bias in social judgments.," *The Journal of neuroscience : the official journal of the Society for Neuroscience*, Vol. 33, pp. 15466–76, Sept. 2013.

89. Kheradmand, A., A. Lasker, and D. S. Zee, "Transcranial Magnetic Stimulation (TMS) of the Supramarginal Gyrus: A Window to Perception of Upright.," *Cerebral cortex (New York, N.Y. : 1991)*, pp. bht267–, Oct. 2013.

90. Gazzaley, A., J. Rissman, J. Cooney, A. Rutman, T. Seibert, W. Clapp, and M. D'Esposito, "Functional interactions between prefrontal and visual association cortex contribute to top-down modulation of visual processing.," *Cerebral cortex (New York, N.Y. : 1991)*, Vol. 17 Suppl 1, pp. i125–35, Sept. 2007.